Universitäts-Augenklinik Tübingen

Forschungsinstitut für Augenheilkunde

The non-canonical impact of Complement factor H on mTOR signaling and cellular metabolism in retinal pigment epithelium (RPE) cells

Inaugural-Dissertation

zur Erlangung des Doktorgrades

der Medizin

der Medizinischen Fakultät

der Eberhard Karls Universität

zu Tübingen

vorgelegt von

Merle, David Adrian

2023

Dekan:	Prof. Dr. rer. nat. B. Pichler
1. Gutachter:	Prof. Dr. rer. nat. M. Ueffing
2. Gutachter:	Prof. Dr. med. Dr. rer. nat. Florian Sennlaub
3. Gutachter:	Prof. Dr. rer. nat. Marlies Knipper
Tag der Disputation:	25.06.2024

Für Sina

Table of contents

List of figures

List of tables

Abbreviations

4E-BP1	Eukaryotic translation initiation factor 4E-binding protein 1
ABC	Ammonium-bicarbonate
ACN	Acetonitrile
AMD	Age-related Macular Degeneration
ATCC	American Type Culture Collection
B	Complement factor B
Bb	Cleaved Complement factor B
BrM	Bruch´s membrane
C3(H2O)	Spontaneously hydrolyzed C3
C3(H2O)Bb	C3 convertase of the alternative pathway
C3bBb	Membrane-bound C3 convertase
CC	Choriocapillaris
ccRCC	Clear cell renal cell carcinoma
DMEM	Dulbecco's Modified Eagle Medium
DMSO	Dimethyl sulfoxide
DTT	Dithiothreitol
ECAR	Extracellular acidification rate
ELM	External Limiting Membrane
EZ	Ellipsoid Zone
FAZ	Foveolar avascular zone
FDR	False discovery rate
FH	Complement factor H
FH 402H	Complement factor H with histidine at position 402
FH 402Y	Complement factor H with tyrosine at position 402
FHL-1	Factor H-like 1
FI	Complement factor I
FRC	Fructose
GCL	Ganglion Cell Layer

GLC	Glucose
GLN	Glutamine
GSK3	Glycogen synthase kinase-3
hAA	High concentration of amino acids
HL	Haller´s Layer
HPLC	High performance liquid chromatography
HRP	Horseradish peroxidase
IAA	2-Iodoacetamide
INL	Inner Nuclear Layer
IPL	Inner Plexiform Layer
IPL	Immunoprecipitation
iPSC	induced pluripotent stem cells
IZ	Interdigitation Zone
MNV	Macular neovascularization
MS	Mass-spectrometry
mTOR	Mechanistic target of rapamycin
mTORC1/2	mTOR complex 1/2
MTT	3-(4,5-dimethylthiazol-2-yl)-2,5-diphenyltetrazolium bromide
MZ	Myoid Zone
OCR	Oxygen consumption rate
OCT	Optical Coherence Tomography
OCTA	Optical Coherence Tomography Angiography
ONL	Outer Nuclear Layer
OPL	Outer Plexiform Layer
OS	Photoreceptor Outer Segments
OXPHOS	Oxidative phosphorylation
PBS	Phosphate-buffered saline
PR	Photoreceptors
PVDF	Polyvinylidene difluoride
RNFL	Retinal Nerve Fiber Layer

RPE	Retinal pigment epithelium
RT	Room temperature
S6K	p70 ribosomal protein S6 kinase
SDS-PAGE	Sodium dodecylsulfate polyacrylamide gel electrophoresis
SEM	Standard error of the mean
siCFH	CFH-silenced cells
siNeg	Non-silenced cells (treated with scrambled siRNA)
SL	Sattler´s Layer
TBST	Tris-buffered saline with tween
TBST	Tris-buffered saline
TFA	Trifluoroacetic acid
UPS	Ubiquitin-proteasomal system
WTD	Western-type diet

1 Introduction

1.1.1 From bacteria to humans: the evolutionary path to the vertebrate retina

The ability to functionally interact with electromagnetic radiation emerged early in evolution. Cyanobacteria were among the first species to develop sophisticated molecular structures that were able to absorb electromagnetic radiation and convert it into chemical energy equivalents. The fact that these bacteria made use of electromagnetic radiation with similar wavelengths to those that humans and other animals are able to visually detect, is to be explained by the fact that electromagnetic radiation with higher energy, like for example ultraviolet radiation or x-rays, would damage the cellular apparatus and lower energy radiation, like for example infrared radiation, would not suffice to provide the needed energy. Therefore, the VIS-spectrum can be seen as a sweet-spot, providing enough energy, yet not causing extensive damage to the cell.

According to the endosymbiont theory, these light-utilizing cyanobacteria were later ingested by larger unicellular organisms, entered a symbiotic relationship and became what we today know as plastids, including the plant´s chloroplasts (1). The widespread distribution of cyanobacteria and plastids allowed for large-scale production of beta-carotene, an essential intermediate for the production of other light-sensitive molecules like retinal and related molecular species (2). In combination with suitable proteins and protein complexes, these molecules conferred the ability to efficiently make use of the sun´s light and improved the evolutionary fitness of the harboring species. While there was a plethora of possible combinations between light-sensitive molecules and associated proteins, retinal derivates combined with opsins outcompeted most of the other possible pairs and became the predominant photosensitive molecular apparatus. With this, the foundation for the evolutionary development of the more sophisticated light-sensing structures was made and a first step towards the human eye as we know it today was taken.

In following periods, multicellular organisms formed accumulations of light-sensitive cells that constituted a so-called eyespot, which enabled to sense the presence or absence of light. A simple eyespot, however, was insufficient to provide directional information and did not allow a light-utilizing organism to actively locomote to well-lit areas. This changed with the development of eyecups, where light-sensitive cells lined a concave indentation and the angle of incoming light defined which set of cells were directly illuminated. With successive protrusion of the eyespot walls, a pinhole-like structure was formed, leading to improved spatial resolution. Later, those simple pinhole-camera-like eyes evolved adnexa like corneas, lenses or extraocular muscles that allowed higher-level vision and superior spatial orientation. From here, neuronal structures developed that allowed for binocularity and the partially decussated chiasm, where parts of the visual information from each eye are transmitted to both hemispheres of the brain, evolved (3).

Not only the overall anatomy of the eye was subject to change, but also the retina itself developed into a highly complex tissue composed of several different cell-types that interact in a tightly orchestrated manner. From an engineer´s point of view, the architecture of the vertebrate retina does not make immediate sense, as the photoreceptive cells are located the furthest away from the incoming light. This fact is testament to the influence of environmental factors on natural selection and the course of evolution, where subtle changes develop over long periods of time and follow the principle of an untargeted bottom-up design process rather than a rational top-down approach (4). Although arguments for the necessity of this inverted organization were made, the cephalopod eye, where the retina shows an everted organization with photoreceptors directly facing the incoming light, clearly demonstrates the opposite (5). Nevertheless, the human retina depicts one of nature´s most sophisticated and arguably most fascinating tissues, which´s complex inner workings are still far from being completely understood.

1.1.2 The anatomy and cells of the human retina

The human retina is embedded in a functional complex that comprises several tissues, each of which fulfills essential functions that in combination enable us to see. The retinas of a group of higher-order primates and the human retina possess a unique architecture with the central area showing a characteristic structure known as the macula (Figure 1). The macula is anatomically defined as a central, round area at the posterior pole that enables high-resolution central vision. It can be subdivided into the perifovea, parafovea, fovea, foveola and the umbo (Figure 1) (6).

The arguably most important retinal cell type, the photoreceptors (PR), detect the incoming photons and convert those to electric stimuli in a process known as phototransduction. PRs comprise two distinct cell types known as rods and cones. While rods are highly light-sensitive and responsible for scotopic vision, i.e., vision in low light conditions, cones are less light-sensitive and confer color vision in photopic, i.e. well-lit, and mesopic, i.e. moderately lit, conditions. At their base, PRs are in close contact with the retinal pigment epithelium (RPE), that not only recycles the shed photoreceptor outer segments but also provides waste disposal and nutrient supply to the PRs. The RPE itself lies above the collagen- and elastin-rich Bruch´s membrane (BrM) followed by a layer of densely packed vessels known as the choriocapillaris (CC). The CC is part of a larger vessel-rich tissue known as the choroid, that feeds the RPE and the outer parts of the retina. On the other side, the PRs are synaptically connected to a specialized neurons known as horizontal and bipolar cells. Horizontal cells provide connections between individual photoreceptors and allow for early signal integration and simple computational processes. Bipolar cells are perpendicularly oriented to the layer of photoreceptors and serve to transmit signals from the PRs to the ganglion cells, which are specialized neurons with long axons that collectively form the optic nerve. On the level of synaptic connections between bipolar and ganglion cells, another cell type, known as amacrine cells can be found. Amacrine cells form connections between different pairs of bipolar and ganglion cells and again enable signal integrational and simple computational

processes. Besides the neuronal cells, that are directly involved in signal transmission and modulation, the proper functioning of the retina is obligatorily dependent on another cell-type known as Müller cells or Müller glia. Müller cells fulfill tasks typical for glial cells, span most of the retina and their footplates form the internal limiting membrane (ILM), which separates the retina from the vitreous, as well as the external limiting membrane (ELM), which separates the PR nuclear bodies form the PR inner and outer segments.

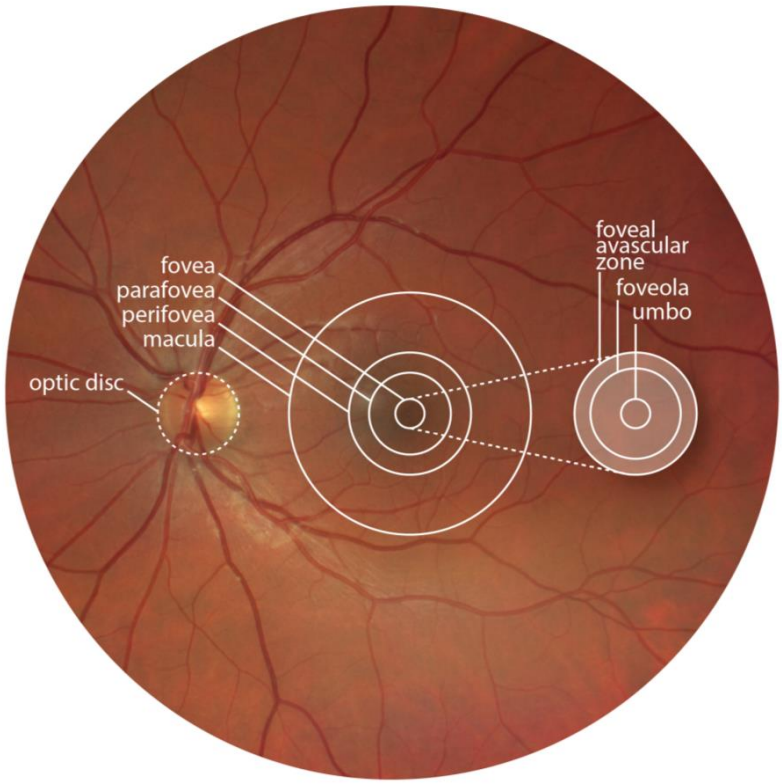

Figure 1: Fundus anatomy and the structure of the macula. The posterior pole of the human eye comprises the optic disc, the vascular arcades and the macula. The optic disc is where retinal nerve fibers, i.e., the axons of the ganglion cells, pierce the sclera and jointly form the optic nerve, which transmits electric signals from the eye to the brain. The macula is the most central area of the retina with a characteristic concentric architecture that includes the parafoveal area, the perifoveal area and the fovea. The fovea itself holds the highest density of photoreceptors and is essential for high-resolution central vision. Within the fovea there is an area devoid of retinal vasculature known as the foveal avascular zone (FAZ) where all the nutrients must be supplied by the choriocapillaris. The fovea is further divided in foveola and umbo with the latter being the most central part. Figure adapted from the one published in (6).

1.1.3 The retina from a clinical perspective

The clinical assessment of the retina is routinely done *via* funduscopy, a technique in which the physician uses a magnifying lens in combination with a bright light to visualize the posterior pole of the eye. The typical funduscopic image allows the examination of the optic disc, retinal vessels as well as the central and peripheral retina (Figure 1). Retinal examination was revolutionized with the emergence of optical coherence tomography (OCT) technology, that uses low-coherence interferometry to generate topographic images of the retina. Most importantly, OCT is completely non-invasive and the generated high-resolution topographical images largely facilitate diagnosis and monitoring of progression in numerous ocular conditions. The layered structures apparent in state-of-the-art OCT images closely resemble the structures to be found in histologic specimens (Figure 2) and therefore offers the unique opportunity to study ocular micro-anatomical phenomena in living tissue (7). Recently, OCT angiography (OCTA) entered the clinical routine and offers high resolution images of the retinal vasculature without the reliance on intravenous injection of fluorescent dyes like in fluorescein and indocyanine green angiography. While OCT-based techniques offer superior axial resolution, lateral resolution is largely limited due to wavefront aberrations caused by micro- and macroscopic imperfections present in the optically relevant structures of the eye. To overcome this limitation, adaptive optics (AO) has recently been introduced in the field of ophthalmology. AO technology was initially used in astronomy to improve the lateral resolution in earth-bound telescopes by correcting wavefront aberrations introduced by atmospheric turbulences via deformable mirrors controlled by a wavefront sensor. AO has since been combined with several other imaging modalities, including for example OCT (AO-OCT), flood illumination imaging (AO-FIO) or scanning laser ophthalmoscopy (AO-SLO). These technologies have enabled visualization of single retinal cells, vessels and associated structures in living eyes. Even though AO-based studies covering a wide range of retinal conditions have been published, we still lack large scale data on healthy controls and standardized analysis protocols. This in combination with the significant costs and time-consuming nature of the technique

is keeping AO from being introduced into clinical routine. Nevertheless, the ability to view single cells in living tissue and advancements in AO-technology will significantly impact on our understanding of retinal health and disease in the future.

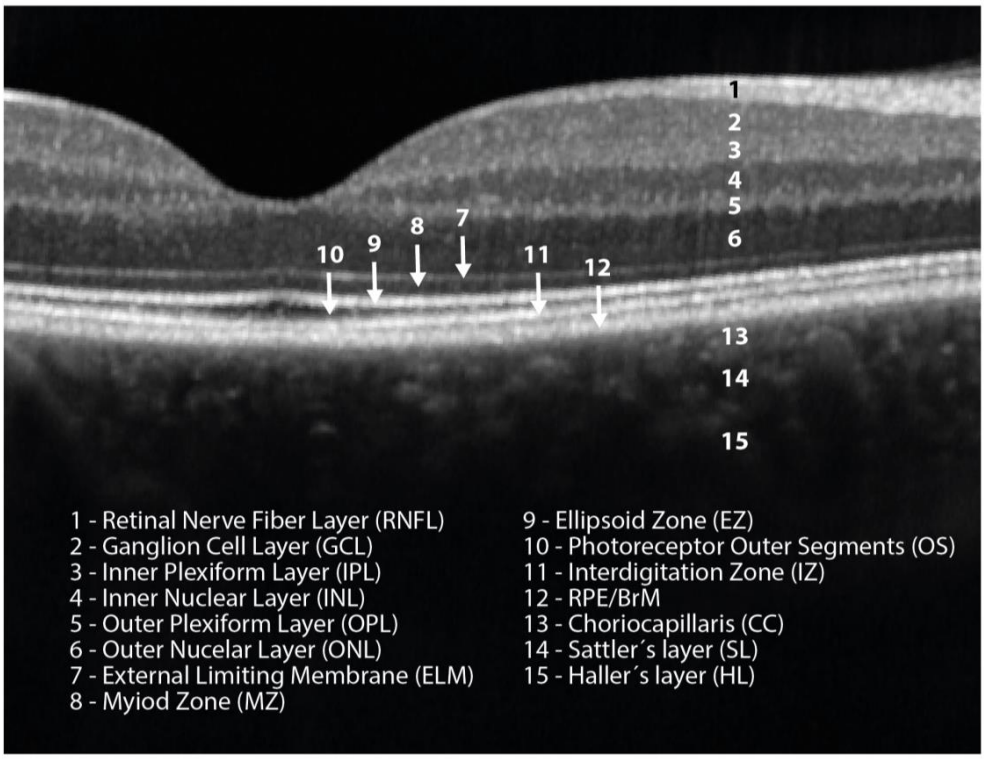

Figure 2: Optical Coherence Tomography (OCT) scans and retinal layers. OCT is a non-invasive, cost-efficient and quick way to visualize the structures of the posterior pole. In macula scans, a typical multilayered pattern can be seen, which´s layers closely resemble the cellular structures identifiable in histologic sections. The innermost layer is the Retinal Nerve Fiber Layer (RNFL), which holds the axons of the ganglion cells. The nuclear bodies of the ganglion cells are found in the next layer, the Ganglion Cell Layer (GCL). The synaptic connections between ganglion cells and bipolar cells form the Inner Plexiform Layer (IPL) and the nuclear bodies of the bipolar, horizontal and amacrine cells can be found in the Inner Nuclear Layer (INL). The synaptic connections between bipolar cells and PRs can be found in the Outer Plexiform Layer (OPL). The nuclear bodies of rod and cone PRs are located in the Outer Nuclear Layer (ONL). The External Limiting Membrane (ELM) is made of müller cell footplates and separates the PR nuclear bodies form the inner and outer segments. The Myoid Zone (MZ) represents the PR inner segments, while the Ellipsoid Zone (EZ) marks the junction between inner and outer segments. The EZ is followed by the PR Outer Segments Layer (OS). The Interdigitation Zone (IZ) is the area where RPE and PRs are in close connection and the RPE cells sheath the PR tips. The complex of RPE and BrM are found in the layer below, connecting to the first layer of the choroid, the choriocapillaris (CC). With increasing distance to the RPE/BrM complex the diameter of the vessels increases, giving rise to Sattler´s Layer (SL), which holds medium-sized vessels, and to the Haller´s Layer (HL), which holds larger vessels.

1.1.4 Molecular aspects of the human macula

The specialized architecture of the macula is reflected on a cellular and molecular level. In general, the density of PRs increases from the retinal periphery towards the center with a maximum in the foveal area. While the peripheral retina is rich in rods and poor in cones, the fovea almost exclusively holds cones (Figure 3). As shown in Figure 2, the layers above the foveal PRs are radially shifted towards the periphery, thereby forming the typical foveal depression and leaving the PRs as the only cells in this area. The outer segments of the foveolar PRs are elongated, resulting in the characteristic dome-like shape in the OCT. This set-up can be viewed as an evolutionary mean to maximize the amount of light that reaches the foveolar PRs, improve the central visual acuity and compensate for the inverted architecture of the vertebrate retina. While this spatial organization improves central vision, it has to be considered an evolutionary compromise as it obligatorily demands absence of retinal vessels (FAZ; Figure 1) and completely relies on the RPE to provide nutrient supply and waste disposal to the cells of the fovea. To accomplish this demanding task, the RPE cells in general, but especially the ones below the fovea, must be highly resistant to all kinds of molecular stressors and hold a high degree of metabolic activity.

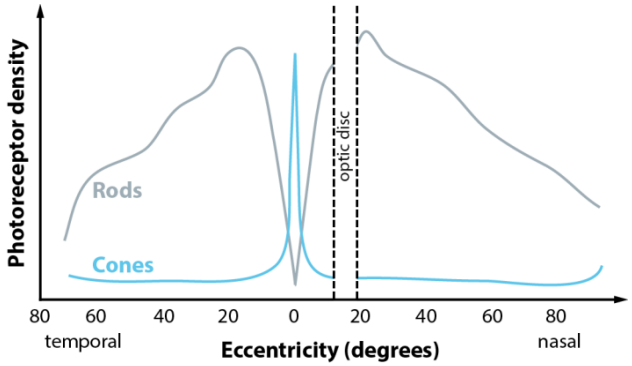

Figure 3: Retinal distribution of rod and cone photoreceptors. While the peripheral retina is rich in rods but poor in cones, the central retina has highest density of cones with a very limited amount of rods. The optic disc does not hold any PRs and is therefore not able to sense light. It is therefore often referred to as the blind spot. Figure adapted from the one published in (8).

The RPE-PR interface is highly specialized and a high interdependency exists between both cell types. Physiologically, RPE forms the outer blood-retina barrier and is solely responsible for molecular trafficking between the choriocapillaris and the neuroretina. Therefore, the RPE cells show a delicate polarization with a distinct set of channels and transporters in their apical and the basal plasma membrane. Physiologically, glucose from the fenestrated capillaries of the CC diffuses through BrM and is shuttled into the RPE cell via specific transporters. From there, most of the glucose is transported through the apical plasma membrane and subsequently taken up by the PRs. Intriguingly, as illustrated in the famous work of Otto Warburg (9), the PRs behave much like cancerous cells when it comes to carbohydrate metabolism. Even in presence of sufficient amounts of oxygen, PRs perform anaerobic glycolysis and secrete the generated lactate. Caution is to be taken when considering the proper terminology here. While Warburg used the term aerobic glycolysis to describe the fact that glucose is converted to lactate even in presence of sufficient amounts of oxygen, the term aerobic glycolysis is now commonly used to describe the glycolytic process of pyruvate generation that subsequently fuels the TCA cycle. In turn, anaerobic glycolysis is commonly used to describe the glycolytic process in which lactate is produced. The lactate produced by the PRs is then taken up by RPE cells and used to provide for their own energy demands. As to be expected with this nutritional interplay, RPE cells heavily rely on oxidative metabolism and intact mitochondria. Accordingly, hypoxia alone is sufficient to induce metabolic stress in RPE cells that can lead to PR degeneration (10). Recently, reductive carboxylation was identified as an important pathway in RPE metabolism (11). Reductive carboxylation was first identified as an important salvage pathway in malignant cells with defective mitochondria, that enables the production of important molecular intermediates needed for macromolecular synthesis (12). Hence, the RPE´s high capacity for reductive carboxylation is another example for its uncommon metabolic program that it at least partially shares with malignant cells.

It is to note that although there are metabolic similarities between RPE and malignant cells, the RPE is a post-mitotic tissue and is fundamentally different from malignant cells.

Another crucial function of the RPE is the phagocytosis of shed PR outer segments (OS). Every day, PRs shed around 10% of their OS, that then need to be taken up and be recycled by the RPE cells to provide important intermediates needed for anabolic processes that are essential for retinal homeostasis and health (13). For instance, RPE cells use fatty acids from the ingested OS not only for their own energy demands but have the capacity to efficiently perform ketogenesis. The produced ketone bodies, predominantly ß-hydroxybutyrate, are then transported through the apical membrane to serve as an energy substrate for PRs and other retinal cells (14). Impairment in the RPE´s phagocytic capacity are associated with PR degeneration and was found to contribute to degenerative retinal phenotypes in several experimental models (15). While defective phagocytosis may induce retinal degeneration, also disturbances in subsequent cellular recycling processes have a significant impact on retinal health. Accordingly, defects in autophagy (16), the ubiquitin-proteasomal system (UPS) (17) and lysosomal pathways (18) have been linked to retinal degeneration. Taken together, PR health is essentially dependent on the metabolic well-being of the RPE cells and any impairment in RPE physiology may contribute to PR degeneration and consecutive visual impairments.

1.1.5 Age-related macular degeneration

Age-related Macular Degeneration (AMD) is a degenerative disease of the central retina and is among the leading causes for legal blindness in developed countries, especially among patients over 60 years of age (19–22). Due to demographic changes in western societies and the strong association with age, global AMD incidence is expected to strongly increase with a projected 288 million cases in 2040 (23). AMD itself is a complex, multifactorial condition impacted by a wide range of genetic, lifestyle associated and environmental factors. Dysfunction of the RPE plays a critical role in AMD pathophysiology and is accompanied with degenerative

processes involving the retina, BrM and the CC, ultimately leading to photoreceptor loss and vision impairment.

Clinically, a major hallmark for AMD is the presence of subretinal deposits commonly known as drusen. Drusen are visible as small white-yellowish accumulations in funduscopy and mainly consist of oxidized lipids and proteins (24). It has been suggested that drusen formation plays a role in AMD pathophysiology by limiting the exchange of proteins and metabolites between the RPE and the choroid. However, according to the current classification of AMD (Table 1), the presence of drusen is not necessarily indicative of AMD. Small drusen with a diameter of less than 63µm, also called drupelets, can be found in the ageing retina and are not considered to be of pathological value as long as no RPE pigment abnormalities can be observed. In some patients these drusen enlarge and from medium-sized (≥63µm, <125µm) or large drusen (≥125µm), that are indicative of early or intermediate AMD, respectively (Table 1). The late stages of AMD are classified as either dry AMD or wet AMD with the main discriminatory hallmark being the presence of macular neovascularization (MNV) in wet AMD and its absence in dry AMD (25,26). For a very long time, no approved treatments for dry AMD were available and interventions were limited to life-style modulatory measures (27). Just very recently, pegcetacoplan, an intravitreally injected complement inhibitor, was approved as the first ever treatment for late-stage dry AMD (geographic atrophy; GA) by the FDA, despite suboptimal efficiency in the phase III clinical trials. In contrast, wet AMD is commonly treated with intravitreal anti-VEGF injections and several different approved agents are available. The induced blockage of VEGF signaling decreases vascular permeability, leads to regression of sub- and intraretinal fluid and limits MNV formation. However, anti-VEGF injections must be considered symptomatic interventions that do not resolve the causative pathology. Therefore, patients frequently need regular injections and tend to progress once the treatment is ceased. Furthermore, anti-VEGF injections cannot prevent secondary pathologies frequently

seen after MNV regression, like for example retinal scarring, formation of subretinal fibrotic deposits of development of anti-VEGF-associated GA.

Table 1: Clinical classification of AMD. The table is based on (25) and was adapted from the table published in (28).

Category	Definition
No apparent ageing changes	• no drusen • no pigmentary abnormalities
Normal ageing changes	• only drupelets • no AMD pigmentary abnormalities
Early AMD	• medium drusen (>63 µm but <125 µm) • no AMD pigmentary abnormalities
Intermediate AMD	• large drusen (>125 µm) • any AMD pigmentary abnormalities
Late AMD	• neovascular AMD and/or any geographic atrophy

AMD primarily affects central vision and leads to central scotomas in advanced cases (Figure 4a,b). Metamorphopsia, i.e. distortion of straight lines, is considered an early sign of disease progression and patients at risk are advised to regularly check for visual disturbances using an Amsler grid (Figure 4c,d). Although central vision loss can be partially compensated via eccentric fixation (29), AMD patients experience severe decreases in quality of life and have an elevated risk to develop depressions (30). Taken together, the increasing incidence along with the lack of causative treatments make AMD a significant threat not only for the quality of life of affected individuals but also for health care systems worldwide. In order to develop

new therapeutic options, a detailed elucidation of the pathogenesis is essential and therefore of utmost importance.

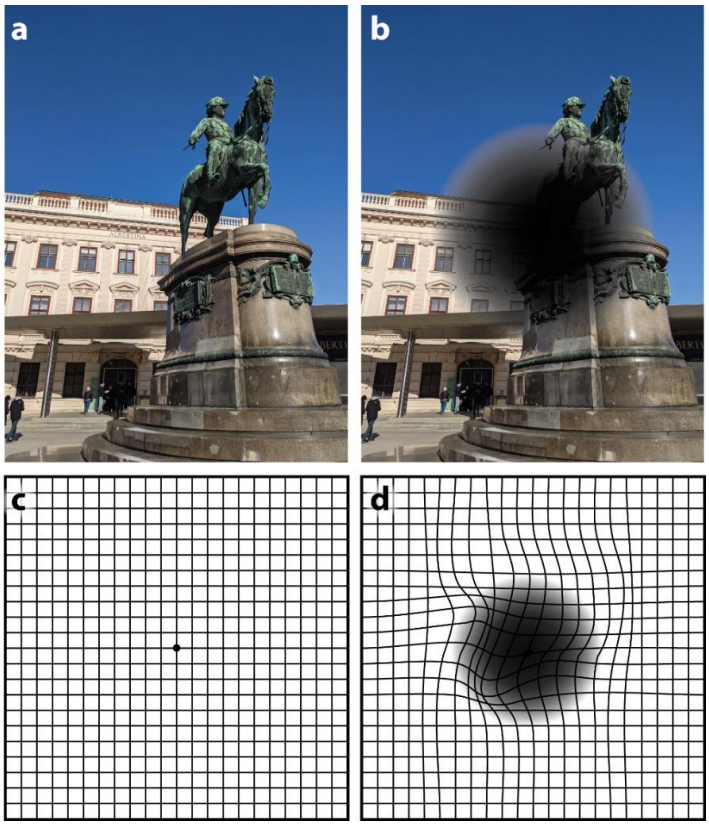

Figure 4: Visual disturbances in AMD. Patients suffering from late-stage AMD frequently experience drastically decreased central vision with pronounced central scotomas. **(a)** Normal view of the scenery without any ocular pathologies. **(b)** Central scotoma with drastically decreased central vision as experienced by patients suffering from advanced stages of AMD. **(c)** Amsler grid as viewed by a person without AMD. **(d)** Amsler grid as viewed by a person suffering from advanced stages of AMD. Metamorphopsia, i.e. distortion of straight lines, and a central scotoma is present.

1.1.6 AMD risk factors

AMD is a complex, multifactorial disease impacted by a wide range of different factors. On one hand, an individual´s age, life-style related factors like smoking or diet and comorbidities, like hypertension or obesity, have a significant impact on disease development and progression (31). On the other hand, genetics play a

prominent role in defining the individual susceptibility for AMD development and progression (32). Early genetic studies found significant association between genetic variants in *CFH* (rs1061170), the gene coding for Complement factor H (FH) (33) and chromosomal region 10q26, which comprises the genes *AMRS2*, coding for a small protein with unclear function, *HTRA1*, that codes for the extracellular matrix (ECM) modifying serine peptidase HtrA1(34) and *PLEKHA1*, coding for a membrane-bound protein with putative role in signal transduction. In 2016, a large genome-wide association study (GWAS) was able to identify 52 genetic variants mapping to 34 loci, that were independently associated with AMD (35). While confirming *CFH*- and *ARMS2*/*HTRA1*-variants to contribute the most risk, it became evident that AMD-genetics are complex and the interplay between several associated variants and numerous other factors define the cumulative, individual risk for the disease (36). The identified variants mapped to genes with a well-known role in defined molecular pathways, including the complement system, ECM remodeling, lipid metabolism and others (37).

1.1.7 AMD, the complement system and factor H

As already implicated by the GWAS results, AMD development was shown to be associated with inflammation and increased activation of the alternative complement pathway, an important part of the complement system (38–40). The complement system is part of innate immunity and consist of more than 30 plasma proteins that form a proteolytic cascade, which confers defense against invading pathogens or aberrant cells. In this cascade, C3 is a central factor, which´s activation triggers processes that ultimately lead to full complement activation and neutralization of the targeted cell. C3 itself can be activated via three different routes: the classical, the lectin and the alternative pathway. In contrast to the other two, the alternative pathway is spontaneously and constantly activated throughout the body and does not require recognition of any specific, pathogen-associated factors. During alternative complement activation, a thioester-bond in C3 undergoes spontaneous hydrolysis to form C3(H_2O). C3(H_2O) then associates with Factor B (FB), which in

turn is cleaved by Factor D (FD) to form C3(H_2O)Bb, the C3 convertase of the alternative pathway. C3(H_2O)Bb subsequently cleaves C3 into C3a and C3b, from which the latter binds to ECM or cellular surfaces of all kinds and forms the membrane-bound C3 convertase (C3bBb). The resulting peak in local C3b production and deposition on the respective cell surface has the potential to induce complement-mediated cell death, theoretically also on healthy cells. To prevent this, several soluble and membrane-bound complement regulators restrict complement cascade propagation and prevent unintended destruction of host cells (41). One major soluble complement regulator is FH, which physiologically limits complement activation by promoting the disassembly of surface-bound C3bBb and by acting as a co-factor in Factor I (FI) mediated degradation of C3b (39). Noteworthy, *CFH* does not only code for FH but also for a truncated version, known as Factor H-like 1 (FHL-1). FHL-1 lacks the ability to bind FI and therefore is limited to surface bound C3bBb. Given the detrimental consequences of uncontrolled complement activation and chronic inflammation (42), activation of the alternative complement pathway has to be tightly controlled and any dysregulation of the complement regulators can potentially lead to uncontrolled inflammatory responses.

As mentioned, rs1061170, a SNP associated with significantly increased risk for AMD (43), leads to an amino acid substitution of tyrosine at position 402 (position 384 in mature, secreted FH) with a histidine (44). In contrast to FH 402Y, FH 402H lacks the ability to alleviate the damage to RPE cells caused by oxidative stress (45). Furthermore, the Y402H substitution leads to altered binding patterns of FH and FHL1 towards components of the ECM and may therefore directly impact on their ability to regulate complement activation (39).

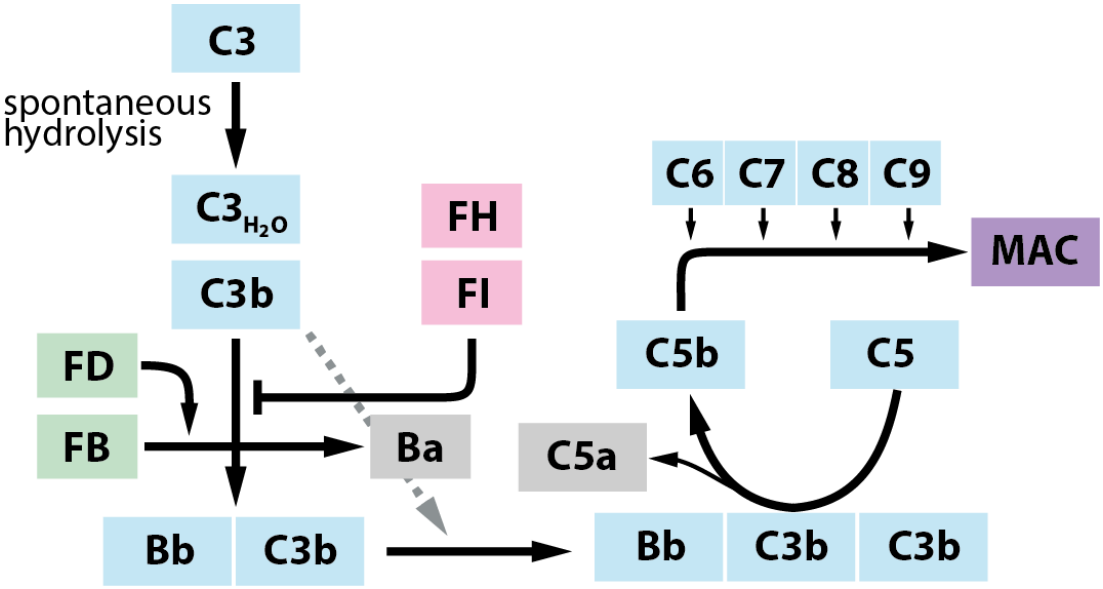

Figure 5: The alternative pathway of the complement system. The alternative pathway of the complement system is activated by spontaneous hydrolysis of C3, resulting in the formation of C3b(H_2O). C3b(H_2O) is bound by Factor B (FB), which is subsequently cleaved by Factor D (FD), giving rise to the C3 convertase of the alternative pathway (C3bBb). The C3 convertase cleaves more C3 into C3b and C3a (not depicted). Additional C3b binds to the C3 convertase and forms the C5 convertase, which in turn cleaves C5 into C5a and C5b. C5b binds C6, C7, C8 and C9 to form the membrane attack complex (MAC). Positive regulators of the complement cascade (FB, FD) are highlighted in green, negative regulators (FH, FI) are highlighted in red.

1.1.8 Non-canonical roles of factor H

While the complement system and its activity is traditionally localized to plasma, studies in T-cells implied the existence of a so-called intracellular complement system, where members of the complement cascade interact with fundamental cellular processes, including cellular metabolism (46). Accordingly, studies in human RPE cells found FH dysregulation to have diverse effects on cellular homeostasis. Besides increased complement turnover as implicated by C3 accumulation, RNAi mediated silencing of *CFH* in hTERT-RPE1 cells lead to significant decreases in glycolysis and cellular respiration as measured by extracellular acidification rates (ECAR) and oxygen consumption rates (OCR) in metabolic flux analyses, respectively. Furthermore, transcriptional dysregulation of several metabolically relevant genes along with genes regulating mitochondrial stability was observed.

Intriguingly, the observed effects were not alleviated by the exogenous supplementation of recombinant FH, pointing towards a distinct role for intracellular FH or at least FH endogenously produced by RPE cells (47). In a subsequent study, *CFH* silencing was also found to increase pro-inflammatory signaling and pro-inflammatory cytokine secretion via the NF-κB pathway. Again, supplementation with recombinant FH was not sufficient to alleviate the observed effects (48). In line with this, the observed mitochondrial deficits were also found in induced pluripotent stem cells (iPSC)-derived RPE cells from AMD patients (49). Likewise, mouse kidney endothelial cells and human glomerular endothelial cells deficient in FH showed decreased cellular respiration and NF-κB upregulation (50). In line with this, clear cell renal cell carcinoma (ccRCC) cells showed cell cycle dysregulation, increased NF-κB signaling and decreased proliferation upon *CFH* silencing (51). In summary, the fact that FH dysregulation leads to similar findings across several cell types points towards a conserved function of endogenous FH. However, mechanistic insights are scarce and further studies are needed to elucidate the non-canonical roles of endogenous FH.

With the observed effects of FH dysregulation on proliferation and metabolism, speculations on affected mTOR (mechanistic target of rapamycin; previously also mammalian target of rapamycin) signaling were made (49). However, no experimental proof of a connection between FH dysregulation and altered mTOR signaling in RPE cells has been published. The mTOR pathway is highly conserved among different species and serves as a central integration hub for a plethora of signals to carefully balance catabolic and anabolic processes by exerting impact on key central cellular processes, like for example autophagy. mTOR itself is a protein kinase that can be found as part of two distinct complexes: mTORC1 and mTORC2. mTORC1 is relevant for cellular metabolism and is promoting processes associated with cellular growth when activated by conditions that imply nutrient availability. In such conditions, mTOR exerts its effects by directly phosphorylating its main downstream effectors p70 ribosomal protein S6 kinase (S6K) and Eukaryotic

translation initiation factor 4E-binding protein 1 (4E-BP1) (52). Indeed, increased mTOR signaling is associated with age-related diseases (53) and mTOR inhibition *via* rapamycin is one of the few interventions capable of limiting ageing effects and contributing to life span extension in several experimental models (54). Given the strong association of AMD with age, mTOR has to be considered an attractive target for future investigations. Intriguingly, functional mTOR complexes are expressed in RPE cells (55) and a transgenic mouse model with increased mTOR activity in the RPE was reported to develop retinal degeneration (56). Furthermore, elevated mTOR activity was detected in RPE cells from AMD patients (57). Taking all this evidence into account, there is an association between altered mTOR signaling and AMD. However, it remains elusive how mTOR activity is affected on a mechanistic level and whether FH dysregulation contributes to this phenomenon.

Therefore, this *in vitro* study aimed to i) analyze mTOR activity in RPE cells upon FH dysregulation, ii) test the therapeutic potency of mTOR inhibition *via* rapamycin and iii) provide mechanistic insights into the role of intracellular/endogenous FH in RPE cells.

2 Material and Methods

2.1 Material

Table 2: Chemicals and reagents

Chemical	Supplier
2-Propanol p.a.	Honeywell, Germany
2-iodacetamide	VWR, USA
Acetonitrile (ACN)	Sigma-Aldrich, USA
Bovine serum albumin (BSA)	Roth, Germany
CAPE	Tocris Bioscience, UK
Chloroform p.a.	Merck, Germany
Complement component C3b	Merck, Germany
Dimethysulfoxid (DMSO)	Roth, Germany
dNTP Mix	Promega, USA
Ethanol p.a.	ITW reagents (AppliChem), Germany
Fetal calf serum (FCS)	Sigma-Aldrich, USA
Glycine	Roth, Germany
HCl 25%	Merck, Germany
iTaq Universal SYBR Green Supermix	Bio-Rad, USA
M-MLV Reverse Transcriptase	Promega, USA
M-MLV RT 5x Buffer	Promega, USA
Methanol p.a.	Honeywell, Germany
Milk powder (non-fat milk)	Roth, Germany
Nuclease-free water	Promega, USA
NuPAGE LDS Sample Buffer	Invitrogen, USA
NuPAGE Sample Reducing Agent	Invitrogen, USA
PageRuler Plus Prestained Protein Ladder	ThermoFisher Scientific, USA
PBS	Sigma-Aldrich, USA
Penicillin-Streptomycin	Life Technologies, USA
ECL Western Blotting Substrate	ThermoFisher Scientific, USA
IP Lysis Buffer	ThermoFisher Scientific, USA
Protease & Phosphatase Inhib. Complex 100x	ThermoFisher Scientific, USA
Protein Assay Dye Reagent	Bio-Rad, USA
PureZOL	Bio-Rad, USA

Random primers	Promega, USA
Rapamycin	Sigma-Aldrich, USA
Roti-Free Stripping buffer	Roth, Germany
Sodium Chloride p.a.	Merck, Germany Sodium
dodecyl sulfate (SDS)	Sigma-Aldrich, USA
Sodium pyruvate	Gibco, USA
Thiazolyl blue (MTT)	Roth, Germany
TriFast	PeqLab Biotechnology, Germany
Trifluoracetic acid (TFA)	Fluka, USA
Tris ultrapure	ITW reagents, Germany
Trypsin-EDTA	Gibco, USA
Trypsin from porcine pancreas	Serva, Germany
Tween20	Sigma-Aldrich, USA
Lullaby transfection reagent	OZ Biosciences, France

Table 3: Buffers and solutions.

Blocking solution	5% BSA or non-fat milk in TBST (1x)
Running buffer (10x)	Rotiphorese 10x SDS-PAGE; Roth, Germany
Running buffer (1x)	10% (v/v) Running buffer (10x) in dH2O
TBS (10x)	300 mM Tris 1.5 M NaCl in ddH2O (pH=7.4)
TBST (1x)	10% (v/v) TBS (10x) 0,1% (v/v) Tween20 in dH2O
Transfer buffer (10x)	1.92 M Glycine 250 mM Tris in ddH2O
Transfer buffer (1x)	10% (v/v) Transfer buffer (10x) 20% (v/v) Methanol in dH2O
80/5 solution	80% (v/v) ACN 5% (v/v) TFA

50/5 solution	80% (v/v) ACN 5% (v/v) TFA
0/5 solution	5% (v/v) TFA

Table 4: Cell culture media.

Medium	**Supplement**
Full medium	DMEM with phenol red Penicillin/Streptomycin (1%) FCS inactivated (10%)
Full medium without phenol red	DMEM without phenol red Sodium pyruvate 100mM (1%) Penicillin/Streptomycin (1%) FCS inactivated (10%)
Serum free medium (SFM)	DMEM without phenol red Sodium pyruvate 100mM (1%) Penicillin/Streptomycin (1%)

Table 5: siRNAs

Target	**Supplier**	**Sequence**
CFH	IDT, USA	5´AUCAUGUGAUAAUCCUUAUAUUCCA 3´ 5´AAGUUCUUUCCUGCACUAAUCACAA 3´ 5´AUGGAAAAAUUGUCAGUAGUGCAA 3´
Negative control	IDT, USA	According to the manufacturer´s recommendations

Table 6: RT-qPCR primers

Gene name	**Forward primer**	**Reverse primer**
CFH	5`- CTG ATC GCA AGA AAG ACC AGT A -3`	5`- TGG TAG CAC TGA ACG GAA TTA G -3`
PINK1	5`- GGC TTG GCA AAT GGA AGA AC -3	5`- CTC AGT CCA GCC TCA TCT ACT A -3
PARKIN	5`- CCA CAC TAC GCA GAA GAG AAA -3`	5`- GAG ACT CAT GCC CTC AGT TAT G -3`
PPARGC1A	5`- AGA GCG CCG TGT GAT TTA T -3`	5`- CTC CAT CAT CCC GCA GAT TTA -3`
GPX1	5`- CAT CAG GAG AAC GCC AAG AA -3`	5`- GCA CTT CTC GAA GAG CAT GA -3`
RPLPO	5`- GGA GAA ACT GCT GCC TCA TAT C -3`	5`- CAG CAG CTG GCA CCT TAT T -3`

Table 7: Primary antibodies for western blotting

Target	Manufacturer	species	Catalogue number
Factor H (FH)	SantaCruz Biotechnology	mouse	sc-166608
Phospho-mTOR (S2448)	Cell Signaling	rabbit	5336
mTOR	Cell Signaling	rabbit	2983
Phospho- S6K (T389)	Cell Signaling	rabbit	9234
S6K	Cell Signaling	rabbit	9202
β-actin	Cell Signaling	mouse	3700

Table 8: Secondary antibodies for western blotting

Target	Manufacturer	species	Catalogue number
HRP-conjugated anti-mouse	Cell Signaling	mouse	7076
HRP-conjugated anti-rabbit	Cell Signaling, USA	rabbit	7074

Table 9: Antibodies for immunoprecipitation

Target	Manufacturer	species	Catalogue number
Complement factor H (FH)	SantaCruz Biotechnology, USA	mouse	sc-166613
unspecific Immunoglobulin G (IgG)	SantaCruz Biotechnology, USA	mouse	sc-2025

Table 10: Hardware and devices

Name	Type	Supplier
Heraeus Fresco 21	Centrifuge	ThermoFisher Scientific, USA
Heraeus MultifugeX3R	Centrifuge	ThermoFisher Scientific, USA
HeraCell 150i	CO2 incubator	Heraeus, Germany
XCell SureLock	Electrophoresis system	Invitrogen, USA
Fusion FX	Imaging camera	Vilber, France

Spark 10M	Microplate reader	Tecan, Switzerland
PrimoVert	Microscope	Zeiss, Germany
AXIO	Microscope	Zeiss, Germany
CFX96 Real-Time System C1000TouchThermal Cycler	Thermocycler	Bio-Rad, USA
Duomax 1030	Platform shaker	Heidolph, Germany
Nanodrop ND-1000	Spectrophotometer	ThermoFisher Scientific, USA
Thermomixer Univortemp	Thermo-Shaker	Universal Labortechnik, Germany
Vortex Genie 2	Vortex Mixer	Scientific industries, USA
Water bath		Memmert, Germany
Mini-Protean Tetra system	Western blotting system	Bio-Rad, USA

2.2 Methods

Parts of this thesis have been published in the peer-review journal *Antioxidants*, under the title “mTOR inhibition via Rapamycin treatment partially reverts the deficit in energy metabolism caused by FH loss in RPE cells” by Merle et al. (58). Relevant passages are specifically referenced.

2.2.1 Cell culture maintenance

hTERT-RPE1 cells, obtained from the American Type Culture Collection (ATCC), were used in all experiments. Cells were cultured in flasks using full medium (see Table 4) and were kept at 37°C in a humidified atmosphere with 5% CO2. Cells were passaged twice per week by a single wash using PBS (Gibco, USA), followed by detachment using 0,05% Trypsin-EDTA (Gibco, USA) and dilution using full medium. For the experiments, the cells were used in between passages 12 to 18.

2.2.2 Experimental setting

Cells were seeded in 6-well plates (300.000 cells/well), 12-well plates (120.000 cells/well) or 24-well plates (60.000 cells/well) using full medium and were allowed to attach overnight. Upon reaching of 60-80% confluence, RNAi-mediated gene silencing was performed. For silencing of *CFH* (from now on referred to as siCFH

cells), a equimolar mixture of three different double strand hairpin RNAs was used and for control conditions (from now on referred to as siNeg cells) a scrambled RNAi was used in the same total concertation. Silencing was performed according to the manufacturer's instructions (Lullaby transfection reagent, OZ Biosciences, France). In all experiments, double stranded siRNAs, obtained from Integrated DNA technologies (IDT, USA), were used (Table 5). After 24h incubation, the medium was removed and exchanged with the experiment-specific medium. After 48h of incubation, cells and supernatants were collected for downstream experimental procedures.

2.2.3 Rapamycin treatment

Rapamycin was dissolved in dimethyl sulfoxide (DMSO) to yield a final concentration of 1mM. Stock aliquots were prepared and kept at -20°C until usage. In experimental conditions using rapamycin, cells were silenced as previously described and 1mM rapamycin stocks were diluted with DMSO to yield 1000x stocks of the respective concentration. 1µl Rapamycin stock per 1ml cell culture medium was used. The final concentration of DMSO never exceeded 0.1%.

2.2.4 MTT assay

Cell viability was assessed using MTT assays in 24-well plates. For rapamycin dose-finding experiments, non-silenced hTRERT-RPE1 cells were used with timing of medium changes mimicking the standard experimental condition. For all other experiments siCFH and siNeg cells were used. After completion of experimental cell culture procedures and incubations, the medium was removed and 500µl MTT solution (1:10 dilution in SFM) was added to each well. After 2h incubation at 37°C, the MTT solution was carefully removed without disintegration of the cell layer and 300µl of lysis solution was added to each well. After a 10min incubation at room temperature (RT) on a platform shaker, the absorption at 590nm was measured.

2.2.5 Protein extraction and SDS-PAGE sample preparation

Proteins were extracted from 1) cell culture supernatants and 2) cell pellets. All samples were kept on ice throughout all procedures. All lysis buffer (Pierce IP Lysis

Buffer; ThermoFisher Scientific, USA) used was supplemented with protease and phosphatase inhibitors (Halt Protease & Phosphatase Inhibitor Complex; ThermoFisher Scientific, USA) according to the manufacturer´s recommendations.

Collection of supernatants was performed by transferring the supernatants into 2ml tubes and centrifugation (3000g, 5min, 4°C) to remove cell debris. Following centrifugation, the supernatants were removed without disintegration of the debris pellet and transferred to a fresh tube. For protein precipitation, the five-fold volume of ice-cold acetone (-20°C) was added to each sample. After vortexting, the samples were incubated to 1h at -20°C, followed by centrifugation (4500g, 20min, 4°C). Supernatants were carefully discarded and pellets were dried at RT for 10min. Subsequently, 100 µl of lysis buffer (Pierce IP Lysis Buffer; ThermoFisher Scientific, USA) was added to each sample. Pellets were incubated on ice and vortexed periodically until they were properly dissolved. To quantify the protein content, Bradford assays were performed as follows. 1µl of each sample was diluted in 50µl dH_2O and 150µl of a 1:5 diluted Bradford reagent (Protein Assay Dye Reagent Concentrate; Bio-Rad, USA) was added. After 10min incubation at RT, absorption at 595nm was measured using a Spark multimode microplate reader (Tecan, Switzerland). For quantification, each Bradford assay contained a standard dilution series (range 0.5 to 10 mg/ml) using BSA (Roth, Germany) and all samples, including standards, were measured in technical triplicates. Concentration determination was carried out *via* linear regression using Excel (Version 16.0.4266.1001). For all samples, equal amounts of total proteins were combined with NuPAGE LDS Sample Buffer (Invitrogen, USA) supplemented with NuPAGE Reducing Agent (Invitrogen, USA) and volumes were adjusted using dH_2O. The samples were then incubated at 95°C for 10min and stored at -20°C. Remaining cell lysates were stored at -80°C.

For protein extraction from cells, 100 µl of lysis buffer was added to each well immediately after removal of supernatants. Plates were stored at -80°C for a minimum of 1h and subsequently incubated for 20min on a platform shaker at 4°C.

Cells were harvested *via* thoroughly scraping before being transferred to 1.5ml tubes and centrifuged to remove debris (13,000g, 15min, 4°C). Supernatants were transferred into a fresh tube without disintegration of the debris pellets and protein quantification *via* Bradford assay was performed as follows. 1µl of each sample was diluted in 50µl dH_2O and 150µl of a 1:5 diluted Bradford reagent (Protein Assay Dye Reagent Concentrate; Bio-Rad, USA) was added. After 10min incubation at RT, absorption at 595nm was measured using a Spark multimode microplate reader (Tecan, Switzerland). For quantification, each Bradford assay contained a standard dilution series (range 0.5 to 10 mg/ml) of BSA (Roth, Germany) and all samples, including standards, were measured in technical triplicates. Concentration determination was carried out *via* linear regression using Excel (Version 16.0.4266.1001). For all samples, 25µg of total protein was combined with NuPAGE LDS Sample Buffer (Invitrogen, USA; 1x final concentration) supplemented with NuPAGE Reducing Agent (Invitrogen, USA; 1x final concentration) and volumes were adjusted to 1µg/µl using dH_2O. Samples were incubated at 95°C for 10min and stored at -20°C. Remaining cell lysates were stored at -80°C.

2.2.6 SDS-PAGE, western blot and detection

SDS-PAGE was performed using precast 8-16% gradient gels (Invitrogen, USA). 25µl of sample were loaded per well and 6µl of pre-stained protein standard was used (PageRulerR Plus Prestained Protein Ladder; ThermoFisher Scientific, USA). Gels were run at 120V for 90min using freshly prepared 1x running buffer (RotiphoreseR SDS PAGE; Roth, Germany). Subsequently, proteins were blotted to a polyvinylidene difluoride (PVDF) membrane previously activated in methanol (Roth, Germany). The transfer was performed in 1x transfer buffer (see Table 3) at 100V for 1h. After transfer completion, membranes were washed twice for 5min in 1x TBST and blocked with 5% dry milk in 1x TBST for 1h at RT. Subsequently, membranes were washed twice with 1x TBST before being placed into 50ml falcon tubes containing 4ml of the respective 1st-antibody dilution (see Table 7). The tubes were incubated at 4°C overnight on a roller, followed by three 15min washes in 1x

TBST. Incubation with the HRP-coupled 2nd-antibody (see Table 8) was performed for 1h at RT on a roller. Membranes were washed twice for 15min in 1x TBST before the western blot detection reagent (Pierce ECL-Western Blotting Substrate, ThermoFisher Scientific, USA) was added to all parts of the membrane. Image acquisition was done using an automatic chemiluminescence imaging system (FusionFX, Vilber Lourmat, France). For stripping, membranes were incubated in stripping buffer (ROTI Free stripping-buffer, Roth, Germany) for 20min at 60°C, followed by two 15min washes in 1xTBST. Re-blocking of membranes was done using 5% dry milk (Roth, Germany) in 1x TBST for 1h at RT and antibody incubations were performed as previously described. After detection of all targets, the membranes were washed once in 1x TBST for 5min and stored at -20°C.

2.2.7 RNA isolation, cDNA synthesis and RT-qPCR

For RNA isolation, cells were grown in 6-well plates. After completion of experimental procedures, cell culture supernatants were removed and processed as described previously. 500µl of RNA isolation reagent (PureZOL, Bio-Rad Laboratories, USA) were added per well and RNA isolation was performed according to the manufacturer´s recommendations. Two washing steps with 70% Ethanol (Roth, Germany) were used. The RNA pellets were carefully dried at RT and re-suspended in 20µl Nuclease free water (ThermoFisher Scientific, USA) by incubation at 56°C for 10min. RNA purity parameters (260nm/280nm- and 260nm/230nm-ratios) and total RNA concentration were measured using a Microvolume UV-VIS Spectrophotometer (Nanodrop ND-1000, ThermoFisher Scientific, USA). Depending on the total amount of RNA retrieved in the respective experiment, 1-5µg of RNA was used for cDNA synthesis. Reactions were run with a total volume of 25µl, including 1µl M-MLV Reverse Transcriptase (200 U/ml), 1µl Random Primers (10 ng/µl), 1µl dNTPs (0.5 mM) and 5µl M-MLV RT 5x Buffer (all reagents for cDNA synthesis were purchased from Promega, USA). The final volumes were adjusted to 25µl using Nuclease free water and the synthesis program included a 10min incubation at 25°C, followed by 1h at 42°C and 10min at 72°C. After completion,

samples were diluted with the 100-fold volume (µl) of used RNA (µg) using Nuclease free water. cDNA preparations were stored at -20°C and remaining RNA samples were stored at -80°C.

For RT-qPCR, primers (all purchased from Integrated DNA technologies, USA) were diluted according to the manufacturer´s recommendations to yield 100µM stocks. Ready-to-use forward and reverse 10µM primer stocks were generated using Nuclease free water. 5µl of cDNA was pipetted to the bottom of each well and 10µl of master mix, including 7,5 µl iTaq Universal SYBR Green Supermix (Bio-Rad, USA), 1,5 µl of the respective primer-mix and 1 µl of Nuclease-free water, was added to each well. Each sample was run in technical duplicates. Reactions were run on a standard qPCR device (CFX96TM Real-Time System, Bio-Rad, USA) and the used 2-step PCR protocol comprised 40 cycles with 5 seconds at 95°C and 30 seconds at 57°C, each. After completion, a melting curve analysis was performed. Gene expression was analyzed *via* the ΔΔCT-method and fold-changes were calculated (fold-change = $2^{-\Delta\Delta CT}$). RPLP0 was used as the housekeeping gene in all experiments.

2.2.8 Seahorse metabolic flux analyses

For metabolic flux analyses, cells were seeded in 6-well plates in full medium without antibiotics. 8-10h after seeding, cells were checked for proper adhesion and RNAi-mediated silencing was performed as described previously. After 24h of incubation, cells were detached using 200µl 0,05% Trypsin-EDTA (Gibco, USA) per well and seeded to 8-well seahorse plates (30,000 cells/well) in full medium without phenol red and incubated for 12h. Subsequently, medium was carefully removed without touching the cell layer and the respective experimental medium was added, followed by an incubation for 48h. All measurements were done using the XFp Extracellular Flux Analyzer (Agilent Technologies, Santa Clara, CA, USA) and all reagents, unless otherwise specified, were purchased from purchased from Sigma-Aldrich, St. Louis, MO, USA. Every condition was run in at least duplicates per plate and results were

normalized to protein content/well using BCA assays (Pierce Biotechnology, Waltham, MA, USA).

For analysis of the oxygen consumption rates (OCR), medium was changed to freshly prepared assay medium (Seahorse XF DMEM Medium, pH=7.4) and three OCR measurements after injection of 1) 10 µM Oligomycin, 2) 10 µM carbonyl cyanide p-trifluoromethoxyphenylhydrazone (CCCP) and 3) 1 µM Antimycin A with1 µM Rotenone were performed within a 15min time frame. The resulting data was analyzed using Wave (Version 2.6) and OCR parameters were calculated (basal respiration, maximal respiratory capacity, respiratory reserve and ATP-linked respiration).

For the analysis of (ECAR), medium was changed to freshly prepared assay medium (Seahorse XF DMEM Medium, pH=7.4) and three ECAR measurements after injection of 1) 10 mM glucose, 2) 10 µM oligomycin and 3) 50 mM 2-deoxy-glucose (2-DG) were performed within a 15min time frame. The resulting data was analyzed via Wave (Version 2.6) and ECAR parameters were calculated (basal glycolysis, glycolytic capacity and glycolytic reserve).

2.2.9 Statistical analysis

Graphs were generated and statistical analyses were run using GraphPad Prism 9 (Version 9.1.1). Normal distribution of data sets was assessed using the Shapiro-Wilk test. To test for significance, paired student t-tests were run for normally distributed data sets, while Mann-Whitney test was used for non-normally distributed data sets. Data are shown as mean with standard error of the mean (SEM). Values were considered significant with a p-value of < 0.05 ($*p < 0.05$, $**p < 0.01$).

2.2.10 Immunoprecipitation, protein digest and Mass-spectroscopy

2.2.10.1 Immunoprecipitation of lysates

500µl of IP lysis buffer was added to each dish immediately after removal of the supernatants. Cells were thoroughly scraped, transferred to fresh tubes and

centrifuged (10,000g, 15min, 4°C) to remove cellular debris. The resulting supernatants were transferred to fresh tubes without disruption of the pellet. For protein quantification *via* Bradford assays, 1µl of each sample was diluted in 50µl dH_2O and 150µl of a 1:5 diluted Bradford reagent (Protein Assay Dye Reagent Concentrate; Bio-Rad, USA) was added. After 10min incubation at RT, absorption at 595nm was measured using a Spark multimode microplate reader (Tecan, Switzerland). For quantification, each Bradford assay contained a standard dilution series (range 0.5 to 10 mg/ml) using BSA (Roth, Germany) and all samples, including standards, were measured in technical triplicates. Concentration determination was carried out via linear regression using Excel (Version 16.0.4266.1001). Equal amounts of total protein were transferred to fresh tubes and adjusted to a total volume of 700µl using IP lysis buffer. 4µg of anti-FH antibody (Santa-Cruz, California, USA) or 4µg of unspecific Immunoglobulin G (IgG; Santa-Cruz, California, USA) were added to the samples and incubated for 1h at 4°C on a roller. 80µl of carefully re-suspended protein G-coupled agarose beads (Protein G PLUS-Agarose beads, Santa Cruz Biotechnology, USA) were added to each sample and incubated at 4°C overnight on a roller. The samples were centrifuged (1000g, 5min, 4°C) and the supernatants were carefully removed without disintegration of the pellet. Afterwards, the pellet was re-suspended in 500µl IP washing buffer, transferred to protein purification columns (35µm receiver columns, Macherey-Nagel, Germany) and washed two more times with 500µl IP washing buffer. Proteins were eluted from the columns using 200µl of glycine buffer and eluates were neutralized by the addition of 20µl Tris buffer. Eluates were stored at -80°C.

2.2.10.2 Protein precipitation and digest

To purify protein, eluates were subjected to methanol/chloroform precipitation. 800µl pure methanol (Roth, Germany) was added to 200µl of eluate in 2ml tubes (Greiner Bio-One, Germany), vortexed thoroughly and centrifuged (9000g, 1min, RT). 200µl of pure chloroform (Sigma-Aldrich, USA) was added to each sample, followed by

thoroughly vortexing and centrifugation (9000g, 1min, RT). Subsequently, 600µl HPLC grade H_2O was added before samples were vortexed thoroughly and centrifuged (16000g, 2min, RT). After phase separation, the upper phase was carefully removed without disrupting the interphase and 600µl of pure methanol were added to each tube. Samples were thoroughly vortexed and centrifuged (16000g, 4min, RT). Supernatants were carefully removed without disrupting the pellet and pellets were dried for 10min at RT. Pellets were stored at -80°C.

For proteolytic digest, the pellets were re-suspended in 30µl of a 50 mM ammonium-bicarbonate solution (ABC solution; Sigma-Aldrich, USA) and 4µl of RapiGest (Waters Corp, USA) were added before vortexing strongly and centrifugation (1000g, 5sec, RT). Afterwards, 1µl of 100 mM Dithiothreitol (DTT; Sigma-Aldrich, USA) was added and samples were incubated 10min at 60°C. After cooling down to RT, 1µl of a 300 mM 2-iodacetamide (IAA) solution (Sigma-Aldrich, USA) was added and samples were incubated for 30min at RT in complete darkness. 1µl Trypsin (Serva, Germany) was added and samples were incubated overnight at 37°C. The next day, samples were centrifuged (9000g, 1min, RT) and the enzymatic digestion was quenched by adding 1.7µl of pure trifluoroacetic acid (TFA; Fluka, USA). Immediately after, the samples were transferred to fresh PP Inserts (Sigma-Aldrich, USA), incubated 10min at RT and centrifuged (16000g, 22°C, 15min). Subsequently, the clear phase was transferred to fresh 0.5ml tubes, followed by peptide purification via StageTips (Proxeon, USA). StageTips were equilibrated with 20µl 80/5 solution (Table 3) and rinsed with 20µl 0/5 solution before the whole sample was loaded. After washing with 20µl 0/5 solution, peptides were eluted into fresh 0.5ml tubes using 20µl 50/5 solution (Table 3) followed by 20µl of 80/5 solution. The volume of the samples was reduced to approximately 5µl by evaporation using a SpeedVac (Thermo-Fisher, USA).

2.2.11 Mass-Spectrometry

The following paragraph has been published in (58). For mass-spectrometric (MS) analysis, sample volumes were adjusted to 15µl using 0.5% (v/v) TFA and 7.5µl of

each sample were used for MS-analysis, while the residual sample volume was stored at -80°C. For MS analysis, an Ultimate3000 RSLC system coupled to an Orbitrap Fusion Tribrid mass spectrometer (Thermo Fisher Scientific, Boston, MA, USA) was used. Peptides were loaded on a nano-trap column (300µm i.d. × 5mm precolumn, packed with Acclaim PepMap100 C18, 5µm, 100Å; Thermo Fisher Scientific, Boston, MA, USA) using a flow rate of 30 µl/min in 0.1% TFA in HPLC grade water for 3min. Subsequently, peptides were eluted and separated *via* an analytical column (75µm i.d. × 25cm, Acclaim PepMap RSLC C18, 2µm, 100Å; Thermo Fisher Scientific, Boston, MA, USA) using a linear gradient from 2% to 30% of buffer B (80% acetonitrile and 0.08% formic acid in HPLC-grade water) in buffer A (2% acetonitrile and 0.1% formic acid in HPLC-grade water) at a flow rate of 300nl/minute over 150 minutes. Remaining peptides were eluted by a short gradient from 30% to 95% buffer B in 10 minutes. MS parameters were as follows: for full MS spectra, the scan range was 335–1,500 with a resolution of 120,000 at m/z=200. MS/MS acquisition was performed in top speed mode with 3 seconds cycle time. The maximum injection time was 50ms. The AGC target was set to 400,000, and the isolation window was 1 m/z. Positive Ions with charge states 2-7 were sequentially fragmented by higher energy collisional dissociation. The dynamic exclusion duration was set to 60 seconds and the lock mass option was activated and set to a background signal with a mass of 445.12002.

2.2.12 Bioinformatic analysis of MS-data

The following paragraph has been published in (58). Analysis of MS data was performed using the MaxQuant (59) software (version 1.6.17.0). Trypsin was selected as the digesting enzyme with maximal 2 missed cleavages. Cysteine carbamidomethylation was set for fixed modifications and oxidation of methionine and N-terminal acetylation were specified as variable modifications. The first search peptide tolerance was set to 20, the main search peptide tolerance to 5ppm. For peptide and protein identification the Human subset of the SwissProt database (Release 2021_04) was used, and contaminants were detected using the MaxQuant

contaminant search. A minimum peptide number of 1 and a minimum length of 6 amino acids was tolerated. Unique and razor peptides were used for quantification. The match between run option was enabled with a match time window of 0.05 min and an alignment time window of 20 min. The statistical analysis including ratio and two sample t-test was done using Perseus (60). Identification of FH potential interactors was performed using a one-sided permutation based t-test with 250 randomizations, an FDR < 0.05 and a S0 of 0.1.

3 Results

Parts of the data and text presented in this thesis have been published in the peer-review journal *Antioxidants*, titled “mTOR inhibition via Rapamycin treatment partially reverts the deficit in energy metabolism caused by FH loss in RPE cells” by Merle et al. (58). Relevant passages are specifically referenced.

3.1 Impact of RNAi-mediated silencing of FH on mTOR activity

To test whether RNAi-mediated silencing of FH leads to elevated mTOR activity, we used SDS-PAGE to assess phospho-protein/total protein ratios of relevant factors.

3.1.1 RNAi-mediated silencing of CFH leads to significantly reduced *CFH* mRNA and FH protein

As a silencing reagent different from previous publications (47,48,61) was used in this thesis, *CFH* silencing (siCFH) efficiency was assessed on the mRNA and protein level relative to controls (siNeg). After optimization of conditions according to the manufacturer´s instructions, *CFH* silencing lead to consistent reductions in mRNA (Figure 6A) and protein levels (**Fehler! Verweisquelle konnte nicht gefunden werden.**Figure 6B) by approximately 80%.

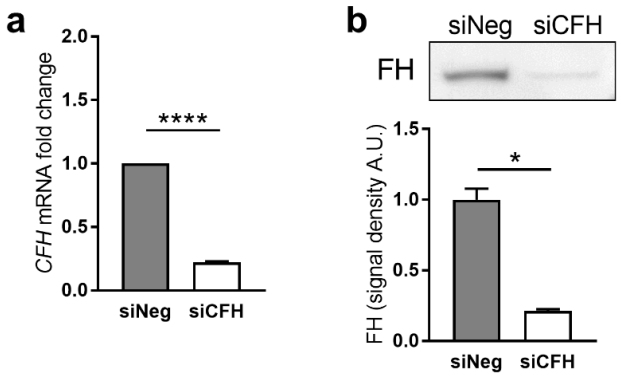

Figure 6: Efficiency of *CFH* silencing in hTERT-RPE1 cells. hTERT-RPE1 cells were silenced for 24 hours with negative control (siNeg) or *CFH* specific (siCFH) siRNA and then incubated for 48 hours. Cell pellets and cell culture supernatants were collected for RNA and protein extraction. a) Evaluation of CFH expression by RT-qPCR analyses. Data are normalized to the housekeeping gene RPLP0 using ΔΔCt methods. SEM is shown, n=4. b) Western blot analyses of FH protein levels in

cell culture supernatants of hTERT-RPE1 cells. Quantification of signal density of 3 independent experiments is shown Significance was assessed by Student's t-test. Figure and figure legend were published in (58).

3.1.2 *CFH* silencing leads to increased mTOR activation

To evaluate the impact of *CFH* silencing on mTOR signaling, comparative western blot analyses were performed. mTOR phosphorylation at serine 2448, a well-established marker for *in vivo* mTOR activity, showed a significantly increased phospho-mTOR/total mTOR ratios in siCFH cells compared to siNeg control cells (**Fehler! Verweisquelle konnte nicht gefunden werden.**Figure 7A). Additionally, the phosphorylation status of threonine 389 in p70 ribosomal protein S6 kinase (S6K), a major downstream effector of mTORC1 and a direct target of mTOR kinase activity, was analyzed. In line with increased mTOR(S2448) phosphorylation, phospho-S6K/total S6K ratios were significantly increased in siCFH cells compared to siNeg control cells (Figure 7B).

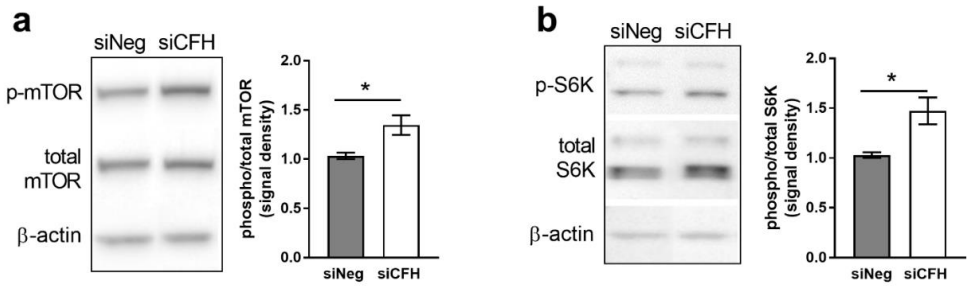

Figure 7: FH knockdown leads to mTOR pathway activation in hTERT-RPE1 cells. hTERT-RPE1 cells were silenced for 24 hours with negative control (siNeg) or CFH specific (siCFH) siRNA and then incubated for 48 hours in the indicated conditions. Cell pellets were collected for protein extraction. a) Western blot analyses of phosphorylated and total levels of mTOR. Total β-actin was used as loading control. Quantification of at least 4 independent experiments is shown, where bars indicate the signal density ratio between levels of phosphorylated and total mTOR. b) Western blot analyses of phosphorylated and total levels of S6K. Total β-actin was used as loading control. Quantification of at least 4 independent experiments is shown, where bars indicate the signal density ratio between levels of phosphorylated and total S6K. SEM is shown. Significance was assessed by Student's t-test. *$p < 0.05$. Figure and figure legend were published in (58).

3.1.3 *CFH* silencing does not significantly alter 4E-BP1 signaling

Besides S6K, Eukaryotic translation initiation factor 4E-binding protein 1 (4E-BP1) is another important downstream effector of mTOR signaling and is directly phosphorylated by mTORC1. Therefore we performed western blot analysis assessing the phosphorylation status of threonine 37/46 (T37/46) in 4E-BP1 (62). The phospho-4E-BP1/β-actin ratios between siCFH and siNeg cells did not show significant differences (Figure 8). It is to note that due to technical reasons, no assessment of total 4E-BP1 levels could be performed and the interpretability of this experiment has therefore to be considered limited.

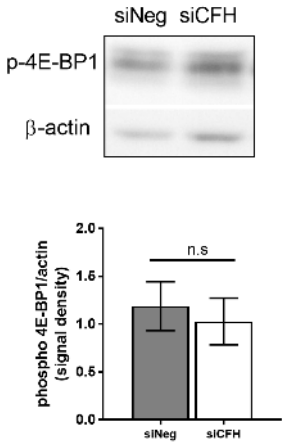

Figure 8: Effects of *CFH* silencing on 4E-BP1 (T37/46) phosphorylation. hTERT-RPE1 cells were silenced for 24 hours with negative control (siNeg) or CFH specific (siCFH) siRNA and then incubated for 48 hours. Cell pellets were collected for protein extraction. Western blot analysis of phosphorylated levels of 4E-BP1 is shown. Total β-actin was used as loading control and quantification of the signal intensity is shown. n=3. SEM is shown, Significance was assessed by Student's t-test. Figure and figure legend were published in (58).

3.1.4 *CFH* silencing does not significantly alter Akt phosphorylation status

As mTOR may be part of distinct complexes, mTORC1 and mTORC2, we wanted to assess the potential impact of *CFH* signaling on mTORC2 activity. Therefore, western blot analyses for the phosphorylation status of Akt (protein kinase B, PKB)

at serine 473 (S473), a well-known target of mTORC2 kinase activity, was analyzed. Although there was a trend towards elevated phospho-Akt/total Akt ratios in siCFH cells compared to siNeg control cells, the differences remained non-significant (Figure 9**Fehler! Verweisquelle konnte nicht gefunden werden.**).

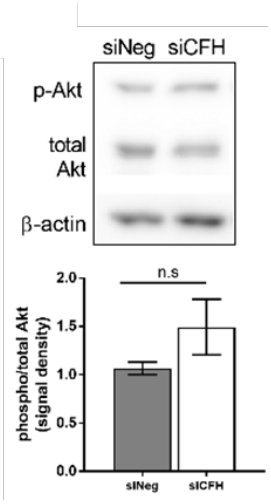

Figure 9: Effects of *CFH* silencing on Akt (S473) phosphorylation. hTERT-RPE1 cells were silenced for 24 hours with negative control (siNeg) or *CFH* specific (siCFH) siRNA and then incubated for 48 hours. Cell pellets were collected for protein extraction. Western blot analysis of phosphorylated levels of Akt is shown. Total β-actin was used as loading control and quantification of the signal intensity is shown. n=3. SEM is shown, Significance was assessed by Student's t-test. Figure and figure legend were published in (58).

3.1.5 *CFH* silencing does not significantly alter GSK3β phosphorylation status

As previous publications showed a significant impact of *CFH* silencing on cellular metabolism, the phosphorylation status of Glycogen synthase kinase 3β at serine 9 (S9) was analyzed *via* western blot. GSK3β (S9) is phosphorylated by Akt, has a central role in metabolic homeostasis and has a proven interrelationship with mTOR signaling. There was no significant difference in phospho-GSK3β/total GSK3β ratios observable between siCFH and siNeg control cells (Figure 10).

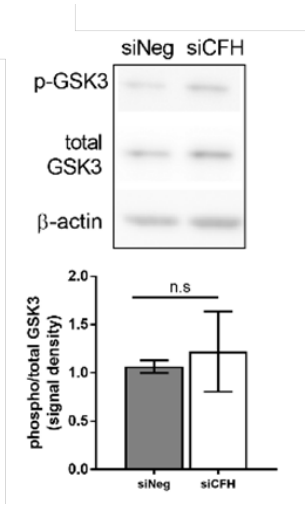

Figure 10: Effects of CFH silencing on GSK3β phosphorylation. hTERT-RPE1 cells were silenced for 24 hours with negative control (siNeg) or CFH specific (siCFH) siRNA and then incubated for 48 hours. Cell pellets were collected for protein extraction. Western blot analysis of phosphorylated levels of GSK3β is shown. Total β-actin was used as loading control and quantification of the signal intensity is shown. n=3. SEM is shown, Significance was assessed by Student's t-test. Figure and figure legend were published in (58).

3.2 Nutritional supplements have limited impact on mTOR activation induced by FH dysregulation

AMD development and progression is linked to western-type diets (WTD) (63). Therefore, we tested the impact of nutritional supplements resembling WTD on mTOR hyperphosphorylation mediated by FH-dysregulation. In control conditions (siNeg), again, a significant upregulation of phospho-mTOR/total mTOR (Figure 11a) and phospho-S6K/total S6K ratios (Figure 11a) were observed. In medium lacking glucose (-GLC) the same trend was observed, although significance was reached only for the phospho-mTOR/total mTOR ratio (Figure 11a), while the phospho-S6K/total S6K ratio remained non-significant with a p-value of 0.06 (**Fehler! Verweisquelle konnte nicht gefunden werden.**Figure 11b). Of all other tested settings, only Fructose containing medium (+FRC) showed a significant upregulation of the phospho-mTOR/total mTOR ratio (**Fehler! Verweisquelle**

konnte nicht gefunden werden.a), while the other conditions yielded similar trends but remained non-significant (Figure 11a,b).

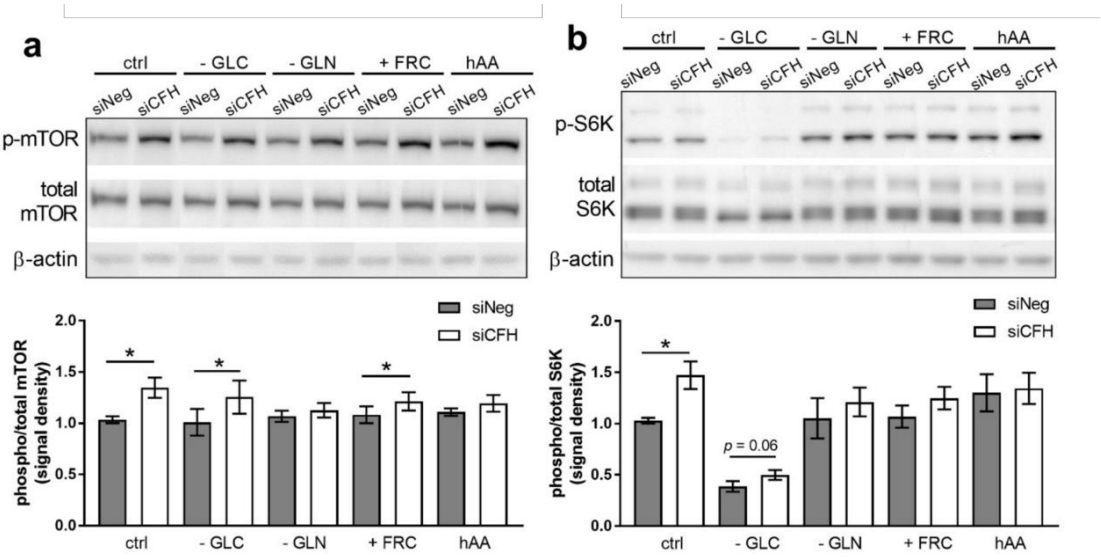

Figure 11: Metabolic supplements have limited impact on mTOR hyperphosphorylation induced by FH dysregulation. The hTERT-RPE1 cells were silenced for 24 h with negative control (siNeg) or *CFH* specific (siCFH) siRNA and then incubated for 48 h in the indicated conditions. Cell pellets were collected for protein extraction. Western blot analyses of phosphorylated and total levels of S6K. Total β-actin was used as loading control. Quantification of at least four independent experiments is shown, where bars indicate the signal density ratio between levels of phosphorylated and total S6K. SEM is shown. Significance was assessed by Student's t-test; * $p < 0.05$. GLC, glucose; GLN, glutamine; FRC, fructose; hAA, high amino acids. Figure and figure legend were published in (58).

3.3 The impact of rapamycin-mediated mTOR inhibition on FH dysregulation-mediated mTOR activation

As shown in previous publications, dysregulation of FH via RNAi-mediated silencing in hTERT-RPE1 cells leads to significant reductions in key parameters of metabolic flux analyses (extracellular acidification rates (ECAR) and oxygen consumption rates (OCR) (47). In the previous chapter, a significant upregulation of mTOR activity was observed upon FH dysregulation. Therefore, we tested the impact of rapamycin-mediated mTOR inhibition on ECARs and OCRs in the same experimental setting.

3.3.1 Low concentrations of rapamycin are sufficient to suppress mTOR-mediated S6K phosphorylation in hTERT-RPE1 cells

To test the effect of rapamycin on mTOR-mediated S6K-phosphorylation, hTERT-RPE1 cells were treated with increasing concentrations of rapamycin (final concentrations 0.1, 1, 10, 100, 200 nM). A strong decrease in S6K phosphorylation was observed with a final concentration of 0.1 nM. Concentrations of 1 nM and above completely abolished S6K phosphorylation while leaving total S6K unchanged (Figure 12).

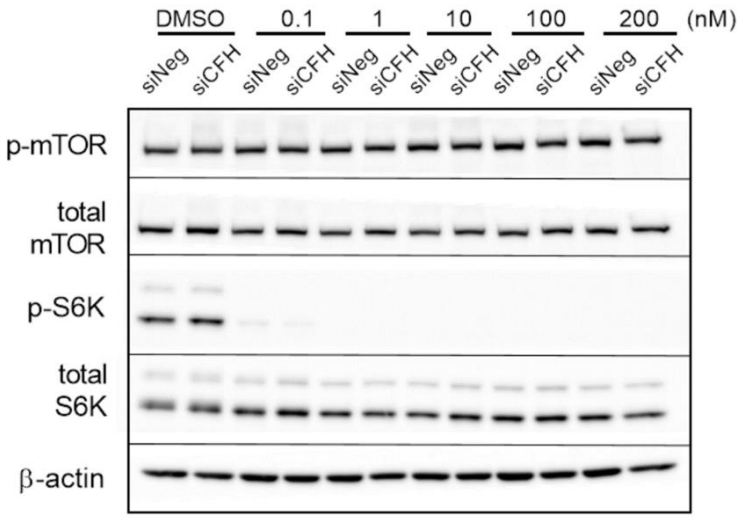

Figure 12: Impact of rapamycin concentration on mTOR activity. hTERT-RPE1 cells were silenced for 24 hours with negative control (siNeg) or *CFH* specific (siCFH) siRNA and then incubated for 48 hours with increasing concentrations of rapamycin as indicated. Cell pellets were collected for protein extraction. Western blot analyses of phosphorylated and total levels of mTOR; phosphorylated and total levels of S6K. Total β-actin was used as loading control. Figure and figure legend were published in (58).

3.3.2 Rapamycin treatment does not significantly alter viability in hTERT-RPE1 cells

To test the impact of rapamycin treatment on the viability of hTERT-RPE1 cells, MTT assays were performed. There was a slight decrease in viability with lower rapamycin concentrations (0.1, 1, 10 nM). However, higher concentrations (100, 200 nM) reached baseline values. Therefore, 200 nM were used in subsequent

experiments as this concentration provided a good balance between solid mTOR inhibition and largely unaltered viability of hTERT-RPE1 cells.

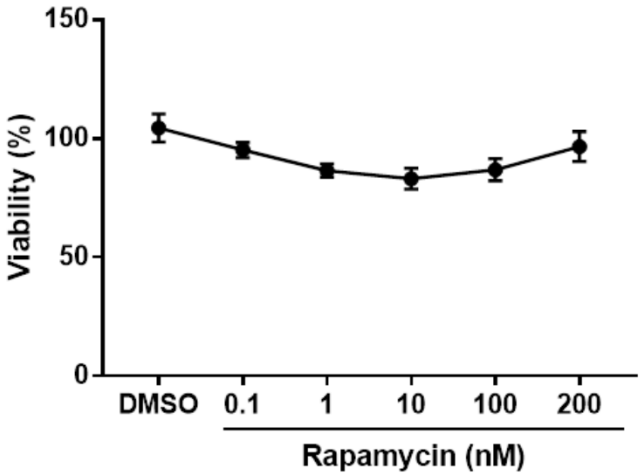

Figure 13: Impact of rapamycin on hTERT-RPE1 viability. hTERT-RPE1 cells were silenced for 24 hours with negative control (siNeg) or *CFH* specific (siCFH) siRNA and then incubated for 48 hours with increasing concentrations of rapamycin as indicated. Viability assessed via MTT assay. N=3. SEM is shown. Figure and figure legend were published in (58).

3.3.3 FH dysregulation leads to decreased extracellular acidification rates that are not rescued by rapamycin treatment

As shown in a previous study (47), FH dysregulation lead to a significant decrease in the ECAR-related parameters glycolytic capacity (Figure 14c) and glycolytic reserve (Figure 14d) with basal glycolysis approaching significance (p=0.06; Figure 14b). Rapamycin treatment did not significantly alter any of the parameters in siNeg or siCFH conditions (Figure 14).

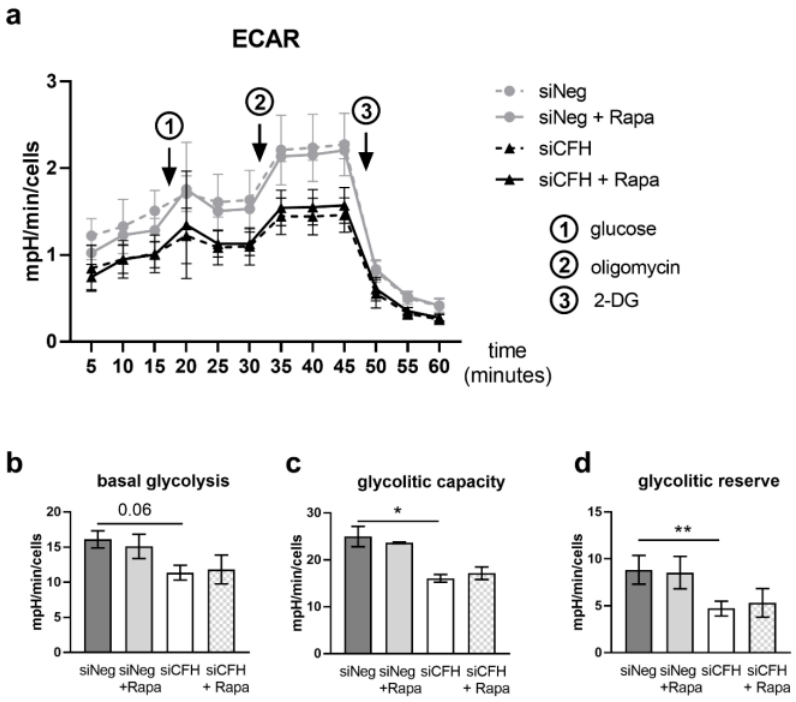

Figure 14: Effect of rapamycin on the glycolytic capacity of hTERT-RPE1 cells. (a) hTERT-RPE1 cells were silenced for 24 hours with negative control (siNeg) or *CFH* specific (siCFH) siRNA, seeded on seahorse plates and incubated in SFM containing 200nM rapamycin or DMSO. Curves represent the extracellular acidification rates (ECAR) measured after 48 hours. SEM shown, n = 5. Arrows indicate injection of glucose (1), oligomycin (2), 2-DG (3). **(b–d)** Parameters of glycolysis were calculated based on the data shown in (a). **(b)** Basal glycolysis, **(c)** glycolytic capacity, **(d)** glycolytic reserve. Significance was assessed by Student's t-test. *p < 0.01. Figure and figure legend were published in (58).

3.3.4 FH dysregulation leads to significantly reduced oxygen consumption rates that are partially rescued by rapamycin treatment

As shown in a previous study (47), FH dysregulation lead to a significant decrease in the OCR-related parameters basal respiration (Figure 15a), maximal respiration (Figure 15b), reserve respiratory capacity (Figure 15c) and ATP-linked respiration (Figure 15d). Here, basal respiration was reduced by 37%, maximal respiration was reduced by 50%, reserve respiratory capacity was reduced by 56% and ATP-linked respiration was reduced by 38%. Rapamycin treatment lead to significant increases in all four parameters when comparing FH silenced (siCFH) with rapamycin-treated

FH silenced cells (siCFH+Rapa) (**Fehler! Verweisquelle konnte nicht gefunden werden.**a,b,c,d). Here, basal respiration was increased by 22%, maximal respiration was increased by 35%, reserve respiratory capacity was increased by 32% and ATP-linked respiration was increased by 25%. Rapamycin treatment did not lead to significant changes in non-silenced (siNeg) cells.

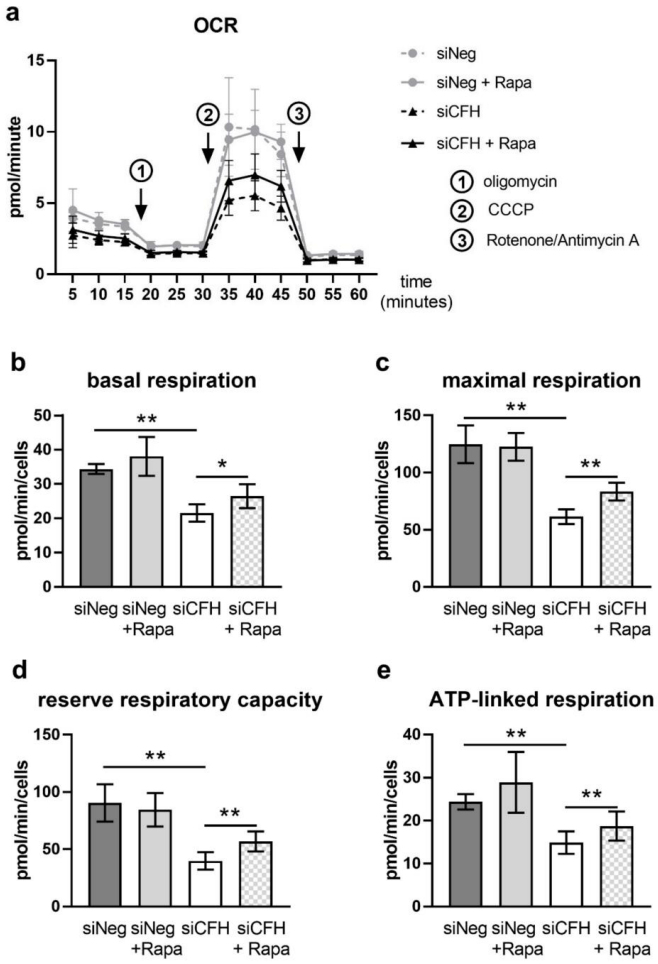

Figure 15: Rapamycin partially rescues FH knockdown-mediated mitochondrial respiration impairment in hTERT-RPE1 cells. (a) hTERT-RPE1 cells were silenced for 24 h with negative control (siNeg) or *CFH* specific (siCFH) siRNA, seeded on seahorse plates and incubated in SFM containing 200 nM rapamycin or DMSO. Curves represent the oxygen consumption rates (OCR) measured after 48 h. SEM shown, n = 4–5. Arrows indicate injection of oligomycin (1), CCCP (2), and antimycin and rotenone (3). **(b–e)** Parameters of mitochondrial respiration were calculated based on the data shown in (a). **(b)** Basal respiration, **(c)** maximal respiration, **(d)** reserve respiratory capacity, and **(e)** ATP-linked respiration. Significance was assessed by Student's t-test; * $p < 0.05$, ** $p < 0.01$. Figure and figure legend were published in (58).

3.4 FH dysregulation-mediated disturbances in gene expression of AMD-relevant genes are reversed by rapamycin-mediated mTOR inhibition

Oxidative stress, mitochondrial damage and impaired autophagy have been linked to AMD (64). Therefore, in a previous study our lab analyzed the expression patterns of a set of representative genes upon FH dysregulation (47). As seen before, genes involved in mitophagy (*PARKIN*, *PINK*), were upregulated upon FH dysregulation. Treatment with rapamycin decreased the expression significantly in FH silenced cells (siCFH) but did not significantly change the expression levels in non-silenced cells (siNeg). While *PARKIN* expression was reduced upon rapamycin treatment but did not reach control values (siNeg+Rapa), the expression of *PINK* completely returned to control value level (Figure 16a,b). Likewise, expression of *PGC1a*, a gene coding for a master regulator of mitochondrial biogenesis and energy metabolism, and *GPX1*, a gene coding for an enzyme essential in redox homeostasis and oxidative stress response, were upregulated upon FH silencing (siCFH). Both genes were significantly downregulated upon rapamycin treatment (siCFH+Rapa) with no significant difference to control cells (siNeg+Rapa) (Figure 16c,d).

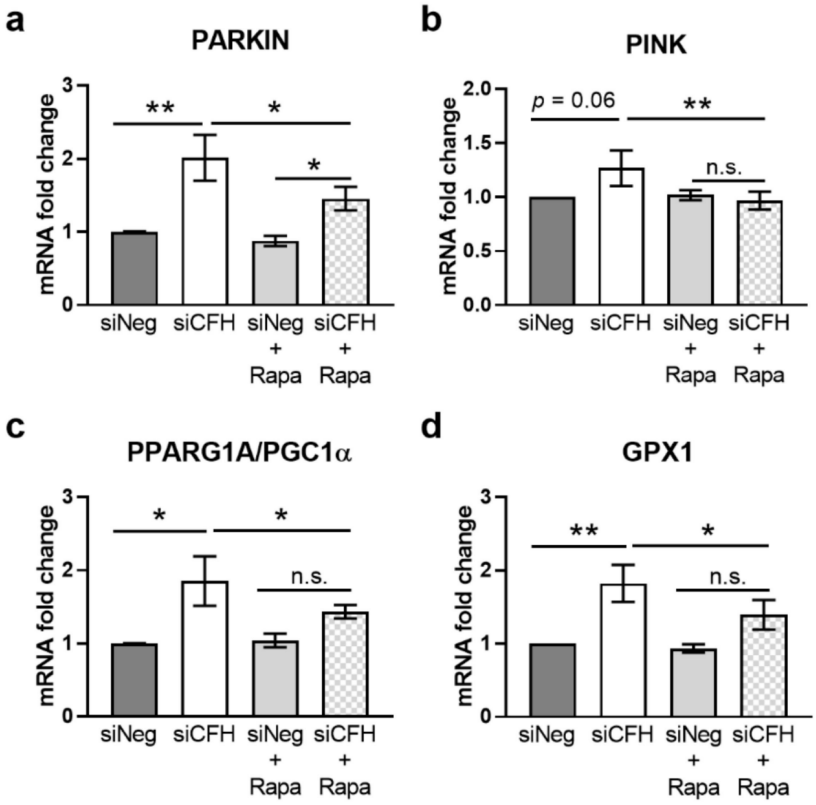

Figure 16: Rapamycin reverts FH knockdown-mediated effects on gene expression. hTERT-RPE1 cells were silenced for 24 h with negative control (siNeg) or *CFH* specific (siCFH) siRNA and then incubated in SFM containing 200 nM rapamycin or DMSO for 48 h. Cell pellets were collected for RNA extraction, cDNA synthesis, and qRT-PCR analyses. **(a)** Evaluation of gene expression levels of E3 Ubiquitin-Protein Ligase Parkin (PARKIN). **(b)** Evaluation of gene expression levels of PTEN induced putative kinase 1 (PINK1). **(c)** Evaluation of gene expression levels of Peroxisome Proliferator-Activated Receptor Gamma Coactivator 1-Alpha (PGC1α). **(d)** Evaluation of gene expression levels of Glutathione Peroxidase 1 (GPX1). Data are normalized to housekeeping gene RPLP0 using ΔΔCt method. SEM is shown, n = 8. Significance was assessed by Student's t-test; * $p < 0.05$, ** $p < 0.01$. n.s. not significant. Figure and figure legend were published in (58).

3.5 Intracellular FH interacts with components of the proteasomal machinery and factors involved in RB1/E2F signaling

The previous experiments showed a clear connection between FH dysregulation and increased mTOR activity and signaling. However, detailed mechanistic insights are still lacking. Therefore, we performed an immunoprecipitation on endogenous FH, followed by a mass-spectrometric analysis of the FH interactome. The experimental

workflow is depicted in Figure 17a. Pathway analysis using the identified interactors revealed cell cycle regulation and the proteasomal pathway as the most significantly associated processes (Figure 17b). Protein-protein interaction-network analysis revealed two distinct, highly significant interaction clusters (Figure 17c). Cluster 1 comprised several factors that are part of the 20S/26S proteasomes (PSMD13, PSME3, PSMB3, PSMB6, PSMA3) and cluster 2 contained several factors involved in RB1/E2F signaling (E2F3, E2F4, RB1, TFDP1, TFDP2).

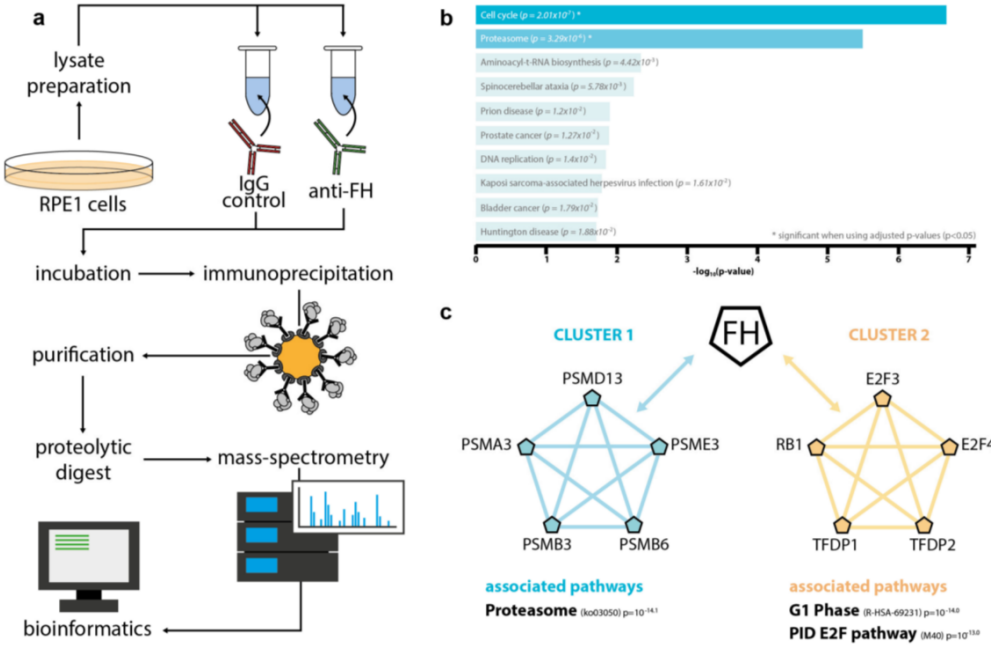

Figure 17: Intracellular FH interacts with factors associated with the proteasomal pathway and the RB1/E2F pathway. The hTERT-RPE1 lysates were incubated with either unspecific immunoglobulin G (control) or anti-FH antibody, and immunoprecipitation was performed using protein-G labeled agarose beads. Proteins were purified and digested with trypsin before mass-spectrometric analysis. **(a)** Experimental workflow. **(b)** Gene-ontology analysis using Enrichr [51] identified the proteasomal pathway and cell cycle as the most represented pathways. **(c)** Protein-protein interaction network analysis via Metascape (65) defined two clusters of FH interacting factors. Cluster 1 included members of the 20S/26S proteasome (PSMD13, PSME3, PSMB6, PSMB3, PSMA3), cluster 2 included factors involved in RB1/E2F signaling and cell-cycle control (E2F3, E2F4, TFDP2, TFDP1, RB1). Figure and figure legend were published in (58).

4 Discussion

Age-related macular degeneration is a growing concern on the individual and the economic level. Despite intensive scientific and clinical efforts, we´re still lacking a detailed pathophysiologic understanding that enables the rational development of efficient treatment strategies. As a complex disease, AMD development and progression is impacted by a plethora of heterogeneous factors. In a modern view, AMD and other complex disease are understood as a disease spectrum with numerous individual but potentially partially overlapping pathologic paths that ultimately lead to a similar clinical manifestation (66). Here, our fundamental assumption is that there are defined subgroups of AMD patients that benefit from individual treatments. However, stratification solely based on genotype has not proven to be sufficient and to date, we are still not able to reliably define specific subgroups. Beyond genetics, future stratification approaches should include but are not necessarily limited to like life-style related aspects and phenotypical properties. While a proper definition of subgroups is an essential step towards rational and sub-group specific therapy development, we also need to unravel the consequences of AMD-associated genetic variants and other associated factors on a molecular level. GWAS studies of the past decades were hugely successful in reproducibly identifying a set of pathways and factors that hold relevance in AMD pathogenesis. However, pathway identification is only a first step in the overall process and detailed molecular analyses are essential to properly define and test potential druggable targets. Strikingly, over 15 years after publication of the biggest GWAS for AMD to date, the vast majority of articles were either reviews or other genetic association studies and only around 19% actually included experimental data (67). Undeniably, genetic association studies will continue to discover new rare variants, define further AMD-relevant pathways and aid stratification approaches. Nevertheless, there is an essential need for us to analyze the molecular consequences of those alterations. Therefore, in this study, we aimed to elucidate the impact of FH dysregulation on cellular metabolism.

The retina and especially the macula is a highly organized and complex tissue made up by numerous cell types with highly specialized morphologies and functions that collaboratively work in a tightly orchestrated manner to enable sight. Fundamental molecular studies are essentially reliant on the availability of suitable experimental models. Unfortunately, it is exceedingly difficult to establish a reliable model for complex tissue like the retina. While simple cell-cultural *in vitro* models are not able to mimic the complex intercellular interplay, establishment of sophisticated multicellular *in vitro* models, like for example retinal organoids, are cost-intensive and time consuming. Those complex models are therefore not well-suited for initial screening experiments that aim to elucidate molecular consequences of a certain aberration on a mechanistic level. Additionally, the fact that the typical macular structure is only present in humans and higher order primates further limits the usability of classic *in vivo* models like for example mice or rats. Therefore, close consideration has to be paid when choosing the experimental model, since different scientific questions rely on different model properties. In this study, we wanted to analyze the molecular impact of FH dysregulation on the mTOR pathway and associated downstream processes. As previous discoveries on the role of endogenous FH were made in hTERT-RPE1 cells (47,48,61), we chose to use the same model for this study. This is justified by the fact that the retinal pigment epithelium (RPE) cells are arguably the primary ocular cell-type affected in AMD pathogenesis. Furthermore, the processes studied are highly conserved pathways that are shared among numerous cell-types, tissues, organs and even species. It is therefore reasonable to assume that findings made in hTERT-RPE1 cells are transferrable to more complex systems. Nevertheless, it is obvious that hTERT-RPE1 cells are by no means sufficient to represent the complex inner workings of the retina and are therefore not to be considered a true AMD model. All findings made in this study will have to be tested in more complex models to validate the disease relevance. Additionally, it is to note that we used RNAi-technology to suppress *CFH* expression, while in AMD, *CFH* is expressed but holds a missense mutation (Y402H) which has proven to limit the physiologic function of the mature

FH protein (68,69). While our experimental set-up does not closely resemble the disease-related state, it undoubtedly allows the study of the fundamental roles of endogenous FH. Intriguingly, recent experiments in our lab using iPSC-derived RPE cells, that harbor the Y402H polymorphism and that are therefore not treated with siRNAs, exhibited the same metabolic disturbances as the *CFH*-silenced hTERT-RPE1 cells used in this study (unpublished data). Taken together, the results of this study are not readily transferrable to the AMD pathophysiology in patients but provide an interesting new link between endogenous FH and mTOR signaling and thus, depict an important cornerstone for future studies.

Experimentally, we chose to monitor mTOR activity *via* western blot-derived phospho-protein/total protein ratios of well-established downstream factors that are direct targets of mTOR. This approach is widely used in biomedical research and is considered the gold standard for in vitro studies (70,71). Based on the fact that we did not observe significantly upregulated levels of Akt (S437) phosphorylation, which is a well-known target of mTORC2 (72,73), we assume that the observed effects are predominantly exerted by mTORC1 activity. The analyzed phosphorylation sites (mTOR S2448, S6K T389, 4E-BP1 T37/46) are established markers for mTORC1 activity (74–76) and are therefore well-suited to analyze mTOR activity in this experimental setting.

In the performed experiments, a consistent hyperactivation of mTOR was observed upon *CFH* silencing as indicated by increased mTOR S2448 and S6K T389 phosphorylation (Figure 7). Notably, 4E-BP1 T37/46 phosphorylation did not show significant differences (Figure 8). While being counterintuitive given that all other mTORC1 markers show upregulation, 4E-BP1 and S6K are known to show differential phosphorylation kinetics (77) and are impacted by a differential set of other factors besides mTOR (78). Furthermore, from a technical perspective, 4E-BP1 blots required extensive incubation times despite thorough protocol optimization and showed less consistent results compared to the other analyzed markers. Taken together, an effect on 4E-BP1 T37/46 was not observed but cannot be completely

ruled out at this point. Further experiments, potentially using other antibodies for 4E-BP1 and 4E-BP1 T37/46 phosphorylation, could help to explain the findings. However, the consistent upregulation found in mTOR S2448 and S6K T389 phosphorylation is sufficient to conclude elevated mTOR activity upon *CFH* silencing. Likewise, we did not observe a difference in GSKβ S9 phosphorylation upon *CFH*-silencing, which does not exclude an effect on mTOR activity as numerous other stimuli may account for that.

The fact that the observed differences in mTOR activity in siNeg vs. siCFH cells were consistent but rather small can potentially be explained by the central role of mTOR signaling within the cell. mTOR, or more specifically mTORC1, is an important signaling hub that integrates numerous cues from an extensive set of different pathways (52). Therefore, the individual impact of a singular pathway or factor that is not a direct modulator of mTOR activity, should be expected to be limited. Additionally, mTOR is an extensively studied factor and the mTOR interactome is well-known (79). FH has not been described as an interactor and therefore the effects mTOR activity exerted by FH dysregulation are very likely to be indirect. However, given the essential role of mTOR in cellular homeostasis even subtle changes can be expected to have profound consequences for the cell, especially in chronic conditions that develop over long periods, like for example AMD. In line with our results, RPE cells from AMD patients were shown to have increased levels of mTOR S2448 and S6K T389 phosphorylation that were qualitatively and quantitatively comparable to our results (57). Furthermore, the gradual build-up of drusen and accumulative cellular damage over time is well in line with small but consistent impairments in cellular physiology and the chronic course of AMD. As mentioned before, drusen – if small in size and present without pigmentary abnormalities in the RPE – are considered physiologic signs of the ageing retina (25). This implies that the underlying processes are the product of subtle but continuous changes in the otherwise heathy but ageing organism, which in turn may be accelerated by accompanying disturbances, like for example dysregulation of FH

physiology. In line with this, increasing mitochondrial dysfunction was seen in RPE of elderly but otherwise healthy subjects and AMD patients, however the latter showed significantly greater decreases over time (80). Additionally, AMD is impacted by a wide range of different factors, like for example smoking or dietary habits. Due to the known association of AMD with western type diets (WTD) (63,81), we chose to test whether increased amounts of typical WTD nutrients (increased amounts of glucose, fructose or amino acids) have an impact on mTOR hyperactivation in normal conditions and upon FH dysregulation (Figure 11). In summary, there were no major effects on mTOR hyperactivation and we assume that nutritional conditions have only a minor impact. In agreement with this, a study using patient-derived iPSCs harboring the FH Y402H variant did not find significant differences between AMD and healthy subjects when modulating the nutritional conditions (49). However, the set of tested conditions has to be considered limited and we cannot exclude important direct effects on the observed processes.

FH dysregulation has been shown to increase the vulnerability of hTERT-RPE1 cells towards oxidative stress and to significantly decreased the capacity for oxidative phosphorylation (OXPHOS) (47). Increased oxidative stress or disruption of OXPHOS were shown to be sufficient to induce RPE dedifferentiation and PR degeneration in the murine retina. Intriguingly, those effects were at least partially mediated *via* the mTOR pathway and treatment with the mTOR-inhibitor rapamycin was sufficient to slow down the degenerative processes (82). Therefore, this study tested rapamycin´s potential to alleviate the detrimental effects caused by *CFH*-silencing. In line with previous experiments in our lab (47), the Seahorse metabolic flux parameters OCR and ECAR were chosen as a primary readout because they showed profound disturbances upon FH dysregulation. In accordance with previous results (47), FH dysregulation resulted in profound reductions in ECAR and OCR (Figure 14&15). Intriguingly, rapamycin treatment partially reversed the effects on OCR (Figure 15) but did not exhibit a relevant effect on ECAR (Figure 14). These findings are well in line with published evidence (82) and are likely to be explained

by the fact that mTOR signaling is not solely carrying the pathologic effects exerted by FH dysregulation. Presumably, the dysregulation is complex and affects several pathways and processes. Hence, mTOR inhibition alone is not sufficient to completely alleviate the pathologic effects exerted by FH dysregulation and a complete rescue would only be possible *via* combinatorial treatments. Intravitreal injection of rapamycin has already been tested in a clinical trial for geographic atrophy (GA) but did not yield positive results (83). However, this trial did not consider the genotype of patients and might have missed positive effects based on a lack of patient stratification. On a more general note, AMD is increasingly understood as a spectrum, with numerous subtypes that may at least partially differ in pathophysiology but present with a similar clinical picture (66). The fact that there is only one approved treatment for dry AMD/GA with suboptimal efficacy highlights the need for a better understanding of AMD and its complex pathophysiology.

FH itself is a well-known plasma-borne modulator of complement activity. The previous finding that exogenous addition of recombinant FH was not able to reverse the pathologic effects of *CFH*-silencing (47,48) points towards a non-canonical role of FH in RPE cells. Likewise, a recent study showed intracellular localization of FH in ccRCC cells and that *CFH*-silencing resulted in decreased proliferation and mortality (51). In order to gather mechanistic information on the intracellular role of FH, MS-based interactome studies were performed. Intriguingly, none of the well-known extracellular FH ligands, like for example HSPG2 or Fibulin-3 (84,85), were found. This can be explained by the fact that the extracellular milieu largely differs from the microenvironment found within the cell and points towards a distinct role of FH within and outside of the cell. Unexpectedly, the two most prominent interaction networks identified within the FH interactome comprised factors involved in the ubiquitin-proteasomal pathway (UPS) and members of the RB1/E2F signaling pathways (Figure 17).

The UPS is a well-orchestrated intracellular system comprising numerous factors that jointly act to enable targeted and tightly controlled degradation of damaged or

unneeded proteins that have been post-translationally modified with ubiquitin (86). Thus, the UPS and autophagy represent two of the most important cellular quality control and recycling pathways. While autophagy is able to clear larger protein aggregates and even whole organelles, the UPS predominantly degrades singular proteins or small protein complexes (87). For a long time, both systems have been thought to act independently from each other. This, however, began to change with the discovery that not only the UPS but also autophagy utilizes monoubiquitination as a molecular signal for targeted degradation (88). Although both systems are not strictly interdependent, recent evidence suggests that there is a relevant interplay. Inhibition of the UPS leads to a compensatory increase in autophagy (89,90) and inhibition of autophagy leads to accumulation of UPS substrates due to p62-mediated UPS inhibition (91). The same interdependency was found in ARPE-19 cells (92). Intriguingly, mTOR inhibition was shown to activate both autophagy and the UPS (93,94). Therefore, mTOR hyperactivation should lead to decreased autophagy and UPS activity in RPE cells, which may have detrimental effects on retinal physiology. Indeed, autophagic markers are reduced in AMD donor eyes compared to healthy controls (95) and decreased autophagy is associated with decreased UPS activity in RPE as implied by the accumulation of ubiquitinated protein species (96). Intriguingly, a study in ARPE-19 cells found decreased *CFH* expression upon UPS inhibition (97) and others have speculated that FH may have a direct impact on the proteasomal activity via the intracellular complement system (49). Although this study is not able to provide definite mechanistic links between FH and mTOR, the interaction with components of the UPS along with dysregulated mTOR signaling strongly implies a regulatory role for intracellular or endogenous FH in RPE cells that is independent from other complement proteins and should therefore be considered non-canonical. While a detailed assessment of those processes was beyond the scope of this study, future experiments should aim to assess the activation status of autophagy and the UPS upon *CFH*-silencing and validate the observed interactions.

The second significantly enriched protein network in the FH interactome included factors involved in RB1/E2F signaling. RB1 itself is a well-known tumor suppressor with an important role in CDK4/CDK6-dependent cell-cycle regulation (98). Beyond cell cycle regulation, RB1 has been implicated in metabolic processes (99) and knockdown of RB1 in hTERT-RPE1 cells resulted in significant reductions in OCR and mitochondrial activity (100). Based on the observed defects in OCR upon *CFH*-silencing, also RB1/E2F signaling depicts an attractive target for future studies. Although, there is no evident link between RB1/E2F signaling and AMD so far, RB1´s impact on cell cycle regulation is of potential interest since cell cycle dysregulation is linked to RPE senescence, which is reported to play a role in AMD pathogenesis (101).

In summary, this study provides evidence for dysregulated mTOR signaling upon *CFH*-silencing and shows that mTOR inhibition via rapamycin is able to partially reverse the defects in cellular respiration. Furthermore, it was the first study to provide data on the intracellular interactome of FH and implies the UPS and RB1/E2F signaling as the main candidate pathways for future studies.

5 Summary

The following summary has been published in (58). Age-related macular degeneration (AMD) is a complex degenerative disease of the retina with multiple risk-modifying factors, including aging, genetics, and lifestyle choices. The combination of these factors leads to oxidative stress, inflammation, and metabolic failure in the retinal pigment epithelium (RPE) with subsequent degeneration of photoreceptors in the retina. The alternative complement pathway is tightly linked to AMD. In particular, the genetic variant in the complement factor H gene (*CFH*), which leads to the Y402H polymorphism in the factor H protein (FH), confers the second highest risk for the development and progression of AMD. Although the association between the FH Y402H variant and increased complement system activation is known, recent studies have uncovered novel FH functions not tied to this activity and highlighted functional relevance for intracellular FH. In our previous studies, we show that loss of *CFH* expression in RPE cells causes profound disturbances in cellular metabolism, increases the vulnerability towards oxidative stress, and modulates the activation of pro-inflammatory signaling pathways, most importantly the NF-kB pathway. Here, we silenced *CFH* in hTERT-RPE1 cells to investigate the mechanism by which intracellular FH regulates RPE cell homeostasis. We found that silencing of *CFH* results in hyperactivation of mTOR signaling along with decreased mitochondrial respiration and that mTOR inhibition via rapamycin can partially rescue these metabolic defects. To obtain mechanistic insight into the function of intracellular FH in hTERT-RPE1 cells, we analyzed the interactome of FH via immunoprecipitation followed by mass spectrometry-based analysis. We found that FH interacts with essential components of the ubiquitin-proteasomal pathway (UPS) as well as with factors associated with RB1/E2F signalling in a complement-pathway independent manner. Moreover, we found that *CFH* silencing affects mRNA levels of the E3 Ubiquitin-Protein Ligase Parkin and PTEN induced putative kinase (Pink1), both of which are associated with UPS. As inhibition of mTORC1 was previously shown to result in increased overall protein degradation via UPS and as FH mRNA

and protein levels were shown to be affected by inhibition of UPS, our data stress a potential regulatory link between endogenous FH activity and the UPS.

Zusammenfassung

Die in der Folge dargestellte Zusammenfassung steht in Anlehnung zur Englischen Zusammenfassung, welche bereits in (58) publiziert wurde. Die Altersbedingte Makuladegeneration (AMD) ist eine komplexe Erkrankung der Netzhaut, welche in ihrer Entstehung durch verschiedene Faktoren, wie beispielsweise Alter, Genetik und Lebenstil, beeinflusst wird. In Kombination bewirken diese Faktoren erhöhten oxidativen Stress, führen zu entzündlichen Prozessen und bewirken metabolische Störungen in den Zellen des Retinalen Pigmentepithels (RPE). In der Konsequenz führen diese Prozesse zur Degeneration der Photorezeptoren in der Netzhaut. Fehlregulationen im alternativen Aktivierungsweg des Komplementsystems sind hierbei eng assoziiert mit der Entstehung der AMD. Insbesondere eine genetische Variante im Komplement Faktor H Gen (*CFH*), welche zur Proteinvariante Y402H in Komplementfaktor H (FH) führt, bringt ein deutlich erhöhtes AMD-Risiko mit sich. Interessanterweise zeigten rezente Studien, dass Varianten in FH nicht nur im extrazellulären Bereich zu Fehlregulation des Komplement Systems führen können, sondern, dass FH auch intrazellular wichtige, nicht Komplement-assoziierte Funktionen hat. In einer vorherigen Studie konnten wir zeigen, dass der Verlust von funktionellem FH in RPE Zellen zu schwerwiegenden Störungen des Zellulären Metabolismus führt, die Vulnerabilität für oxidativen Stress erhöht und Einfluss auf wichtige pro-inflammatorische Signalwege, wie zum Beispiel den NF-kB Signalweg, nimmt. Im Zuge dieser Studie nutzten wir RNAi Technologie um die Expression von *CFH* in hTERT-RPE1 herunterzuregulieren und zu untersuchen in welcher Art und Weise FH die zelluläre Homöstase von RPE Zellen beeinflusst. Im Zuge der Studie konnten wir zeigen, dass ein Herunterregulieren von *CFH* zur Überaktivierung des mTOR Signalweges führt, die mitochondriale Zellatmung verringert und, dass die Inhibition von mTOR mittels Rapamycin in der Lage ist diese metabolischen Effekte zumindest teilweise umkehren kann. Um ein besseres Verständnis über die

intrazellulären Funktionen von FH in hTERT-RPE1 zu erlangen, untersuchten wir in einem nächsten Schritt das intrazelluläre Interaktom von FH mittels endogener Immunprezipitation gefolgt von massenspektrometrischer Analyse der Bindungspartner. Hier zeigte sich, dass FH mit essentiellen Komponenten des Ubiquitin-Proteasom System (UPS) und Faktoren des RB1/E2F Signalwegs in einer Komplement-unabhängigen Weise interagiert. Zusätzliche zeigte sich, dass die Herunterregulation der CFH Expression die mRNA Expression der E3 Ubiquitin-Protein Ligase Parkin und von PTEN induced putative kinase (Pink1), welche beide mit dem UPS assoziiert sind, beeinflusst. In Anbetracht der Tatsache, dass mTOR bekanntermaßen die Proteindegradation über das UPS fördern kann und, dass die *CFH* Expression durch die Inhibition des UPS beeinflusst wird, zeigen unsere Daten eine mögliche regulatorische Verbindung zwischen endogener FH-Aktivität und dem UPS.

6 References

1. Gray MW. Lynn Margulis and the endosymbiont hypothesis: 50 years later. Mol Biol Cell. 2017 May;28(10):1285–7.
2. Sandmann G. Diversity and origin of carotenoid biosynthesis: its history of coevolution towards plant photosynthesis. New Phytol [Internet]. 2021;232(2):479–93. Available from: https://nph.onlinelibrary.wiley.com/doi/abs/10.1111/nph.17655
3. Hoskins SG. Control of the development of the ipsilateral retinothalamic projection in Xenopus laevis by thyroxine: results and speculation. J Neurobiol. 1986 May;17(3):203–29.
4. Novella S. Suboptimal Optics: Vision Problems as Scars of Evolutionary History. Evol Educ Outreach [Internet]. 2008;1(4):493–7. Available from: https://doi.org/10.1007/s12052-008-0092-1
5. Hanke FD, Kelber A. The Eye of the Common Octopus (Octopus vulgaris) [Internet]. Vol. 10, Frontiers in Physiology . 2020. Available from: https://www.frontiersin.org/articles/10.3389/fphys.2019.01637
6. Kim LA, Jacoba C, Patel N. Diabetic Macular Ischemia [Internet]. 2021. Available from: https://eyewiki.aao.org/Diabetic_Macular_Ischemia
7. Staurenghi G, Sadda S, Chakravarthy U, Spaide RF. Proposed lexicon for anatomic landmarks in normal posterior segment spectral-domain optical coherence tomography: the IN•OCT consensus. Ophthalmology. 2014 Aug;121(8):1572–8.
8. Purves D, Fitzpatrick D, Katz LC, Lamantia AS, McNamara JO, Williams SM, et al. Neuroscience [Internet]. Sinauer Associates; 2000. Available from: https://books.google.de/books?id=F4pTPwAACAAJ
9. Warburg O, Wind F, Negelein E. THE METABOLISM OF TUMORS IN THE BODY. J Gen Physiol. 1927 Mar;8(6):519–30.
10. Kurihara T, Westenskow PD, Gantner ML, Usui Y, Schultz A, Bravo S, et al. Hypoxia-induced metabolic stress in retinal pigment epithelial cells is sufficient to induce photoreceptor degeneration. Elife. 2016 Mar;5.
11. Du J, Yanagida A, Knight K, Engel AL, Vo AH, Jankowski C, et al. Reductive carboxylation is a major metabolic pathway in the retinal pigment epithelium. Proc Natl Acad Sci U S A. 2016 Dec;113(51):14710–5.
12. Mullen AR, Wheaton WW, Jin ES, Chen P-H, Sullivan LB, Cheng T, et al. Reductive carboxylation supports growth in tumour cells with defective mitochondria. Nature [Internet]. 2012;481(7381):385–8. Available from: https://doi.org/10.1038/nature10642

13. Kevany BM, Palczewski K. Phagocytosis of retinal rod and cone photoreceptors. Physiology (Bethesda). 2010 Feb;25(1):8–15.

14. Adijanto J, Du J, Moffat C, Seifert EL, Hurle JB, Philp NJ. The retinal pigment epithelium utilizes fatty acids for ketogenesis. J Biol Chem. 2014 Jul;289(30):20570–82.

15. Inana G, Murat C, An W, Yao X, Harris IR, Cao J. RPE phagocytic function declines in age-related macular degeneration and is rescued by human umbilical tissue derived cells. J Transl Med. 2018 Mar;16(1):63.

16. Lin W, Xu G. Autophagy: A Role in the Apoptosis, Survival, Inflammation, and Development of the Retina. Ophthalmic Res. 2019;61(2):65–72.

17. Lobanova ES, Finkelstein S, Li J, Travis AM, Hao Y, Klingeborn M, et al. Increased proteasomal activity supports photoreceptor survival in inherited retinal degeneration. Nat Commun. 2018 Apr;9(1):1738.

18. Rodríguez-Muela N, Hernández-Pinto AM, Serrano-Puebla A, García-Ledo L, Latorre SH, de la Rosa EJ, et al. Lysosomal membrane permeabilization and autophagy blockade contribute to photoreceptor cell death in a mouse model of retinitis pigmentosa. Cell Death Differ [Internet]. 2015;22(3):476–87. Available from: https://doi.org/10.1038/cdd.2014.203

19. Kawasaki R, Yasuda M, Song SJ, Chen S-J, Jonas JB, Wang JJ, et al. The prevalence of age-related macular degeneration in Asians: a systematic review and meta-analysis. Ophthalmology. 2010 May;117(5):921–7.

20. Wong TY, Chakravarthy U, Klein R, Mitchell P, Zlateva G, Buggage R, et al. The natural history and prognosis of neovascular age-related macular degeneration: a systematic review of the literature and meta-analysis. Ophthalmology. 2008 Jan;115(1):116–26.

21. Klaver CC, Assink JJ, van Leeuwen R, Wolfs RC, Vingerling JR, Stijnen T, et al. Incidence and progression rates of age-related maculopathy: the Rotterdam Study. Invest Ophthalmol Vis Sci. 2001 Sep;42(10):2237–41.

22. Bourne RRA, Jonas JB, Bron AM, Cicinelli MV, Das A, Flaxman SR, et al. Prevalence and causes of vision loss in high-income countries and in Eastern and Central Europe in 2015: magnitude, temporal trends and projections. Br J Ophthalmol. 2018 May;102(5):575–85.

23. Wong WL, Su X, Li X, Cheung CMG, Klein R, Cheng C-Y, et al. Global prevalence of age-related macular degeneration and disease burden projection for 2020 and 2040: a systematic review and meta-analysis. Lancet Glob Heal. 2014 Feb;2(2):e106-16.

24. Wang L, Clark ME, Crossman DK, Kojima K, Messinger JD, Mobley JA, et al. Abundant lipid and protein components of drusen. PLoS One. 2010

Apr;5(4):e10329.

25. Ferris FL 3rd, Wilkinson CP, Bird A, Chakravarthy U, Chew E, Csaky K, et al. Clinical classification of age-related macular degeneration. Ophthalmology. 2013 Apr;120(4):844–51.

26. Spaide RF, Jaffe GJ, Sarraf D, Freund KB, Sadda SR, Staurenghi G, et al. Consensus Nomenclature for Reporting Neovascular Age-Related Macular Degeneration Data: Consensus on Neovascular Age-Related Macular Degeneration Nomenclature Study Group. Ophthalmology. 2020 May;127(5):616–36.

27. Ammar MJ, Hsu J, Chiang A, Ho AC, Regillo CD. Age-related macular degeneration therapy: a review. Curr Opin Ophthalmol. 2020 May;31(3):215–21.

28. Salmon J. Kanski's Clinical Ophthalmology E-Book: A Systematic Approach [Internet]. Elsevier Health Sciences; 2019. Available from: https://books.google.de/books?id=HXW7DwAAQBAJ

29. Nilsson UL, Frennesson C, Nilsson SEG. Patients with AMD and a large absolute central scotoma can be trained successfully to use eccentric viewing, as demonstrated in a scanning laser ophthalmoscope. Vision Res. 2003 Jul;43(16):1777–87.

30. Slakter JS, Stur M. Quality of life in patients with age-related macular degeneration: impact of the condition and benefits of treatment. Surv Ophthalmol. 2005;50(3):263–73.

31. Risk factors associated with age-related macular degeneration. A case-control study in the age-related eye disease study: Age-Related Eye Disease Study Report Number 3. Ophthalmology. 2000 Dec;107(12):2224–32.

32. Armstrong RA, Mousavi M. Overview of Risk Factors for Age-Related Macular Degeneration (AMD). J Stem Cells. 2015;10(3):171–91.

33. Klein RJ, Zeiss C, Chew EY, Tsai J-Y, Sackler RS, Haynes C, et al. Complement factor H polymorphism in age-related macular degeneration. Science. 2005 Apr;308(5720):385–9.

34. Iyengar SK, Song D, Klein BEK, Klein R, Schick JH, Humphrey J, et al. Dissection of genomewide-scan data in extended families reveals a major locus and oligogenic susceptibility for age-related macular degeneration. Am J Hum Genet. 2004 Jan;74(1):20–39.

35. Fritsche LG, Igl W, Bailey JNC, Grassmann F, Sengupta S, Bragg-Gresham JL, et al. A large genome-wide association study of age-related macular degeneration highlights contributions of rare and common variants. Nat Genet. 2016 Feb;48(2):134–43.

36. Black JRM, Clark SJ. Age-related macular degeneration: genome-wide association studies to translation. Genet Med. 2016 Apr;18(4):283–9.

37. de Breuk A, Acar IE, Kersten E, Schijvenaars MMVAP, Colijn JM, Haer-Wigman L, et al. Development of a Genotype Assay for Age-Related Macular Degeneration: The EYE-RISK Consortium. Ophthalmology. 2021 Nov;128(11):1604–17.

38. Thurman JM, Holers VM. The Central Role of the Alternative Complement Pathway in Human Disease. J Immunol [Internet]. 2006 Feb 1;176(3):1305 LP – 1310. Available from: http://www.jimmunol.org/content/176/3/1305.abstract

39. Armento A, Ueffing M, Clark SJ. The Complement System in Age-related macular Degeneration. :1–37.

40. Heesterbeek TJ, Lechanteur YTE, Lorés-Motta L, Schick T, Daha MR, Altay L, et al. Complement Activation Levels Are Related to Disease Stage in AMD. Invest Ophthalmol Vis Sci. 2020 Mar;61(3):18.

41. Ferreira VP, Pangburn MK, Cortés C. Complement control protein factor H: the good, the bad, and the inadequate. Mol Immunol. 2010 Aug;47(13):2187–97.

42. Furman D, Campisi J, Verdin E, Carrera-Bastos P, Targ S, Franceschi C, et al. Chronic inflammation in the etiology of disease across the life span. Nat Med [Internet]. 2019;25(12):1822–32. Available from: https://doi.org/10.1038/s41591-019-0675-0

43. Maugeri A, Barchitta M, Agodi A. The association between complement factor H rs1061170 polymorphism and age-related macular degeneration: a comprehensive meta-analysis stratified by stage of disease and ethnicity. Acta Ophthalmol. 2019 Feb;97(1):e8–21.

44. Day AJ, Willis AC, Ripoche J, Sim RB. Sequence polymorphism of human complement factor H. Immunogenetics [Internet]. 1988;27(3):211–4. Available from: https://doi.org/10.1007/BF00346588

45. Borras C, Canonica J, Jorieux S, Abache T, El Sanharawi M, Klein C, et al. CFH exerts anti-oxidant effects on retinal pigment epithelial cells independently from protecting against membrane attack complex. Sci Rep. 2019 Sep;9(1):13873.

46. Liszewski MK, Kolev M, Le Friec G, Leung M, Bertram PG, Fara AF, et al. Intracellular complement activation sustains T cell homeostasis and mediates effector differentiation. Immunity. 2013 Dec;39(6):1143–57.

47. Armento A, Honisch S, Panagiotakopoulou V, Sonntag I, Jacob A, Bolz S, et al. Loss of Complement Factor H impairs antioxidant capacity and energy metabolism of human RPE cells. Sci Rep. 2020 Jun;10(1):10320.

48. Armento A, Schmidt TL, Sonntag I, Merle DA, Jarboui MA, Kilger E, et al. CFH Loss in Human RPE Cells Leads to Inflammation and Complement System Dysregulation via the NF-κB Pathway. Int J Mol Sci. 2021 Aug;22(16).

49. Ebeling MC, Geng Z, Kapphahn RJ, Roehrich H, Montezuma SR, Dutton JR, et al. Impaired Mitochondrial Function in iPSC-Retinal Pigment Epithelium with the Complement Factor H Polymorphism for Age-Related Macular Degeneration. Cells. 2021 Apr;10(4).

50. Mahajan S, Jacob A, Kelkar A, Chang A, Mcskimming D, Neelamegham S, et al. Local complement factor H protects kidney endothelial cell structure and function. Kidney Int. 2021 Oct;100(4):824–36.

51. Daugan M V, Revel M, Thouenon R, Dragon-Durey M-A, Robe-Rybkine T, Torset C, et al. Intracellular Factor H Drives Tumor Progression Independently of the Complement Cascade. Cancer Immunol Res. 2021 Aug;9(8):909–25.

52. Liu GY, Sabatini DM. mTOR at the nexus of nutrition, growth, ageing and disease. Nat Rev Mol Cell Biol [Internet]. 2020;21(4):183–203. Available from: https://doi.org/10.1038/s41580-019-0199-y

53. Xu S, Cai Y, Wei Y. mTOR Signaling from Cellular Senescence to Organismal Aging. Aging Dis. 2014 Aug;5(4):263–73.

54. Johnson SC, Rabinovitch PS, Kaeberlein M. mTOR is a key modulator of ageing and age-related disease. Nature. 2013 Jan;493(7432):338–45.

55. Chen Y, Wang J, Cai J, Sternberg P. Altered mTOR signaling in senescent retinal pigment epithelium. Invest Ophthalmol Vis Sci. 2010 Oct;51(10):5314–9.

56. Huang J, Gu S, Chen M, Zhang S-J, Jiang Z, Chen X, et al. Abnormal mTORC1 signaling leads to retinal pigment epithelium degeneration. Theranostics. 2019;9(4):1170–80.

57. Zhang M, Jiang N, Chu Y, Postnikova O, Varghese R, Horvath A, et al. Dysregulated metabolic pathways in age-related macular degeneration. Sci Rep [Internet]. 2020;10(1):2464. Available from: https://doi.org/10.1038/s41598-020-59244-4

58. Merle DA, Provenzano F, Jarboui MA, Kilger E, Clark SJ, Deleidi M, et al. mTOR Inhibition via Rapamycin Treatment Partially Reverts the Deficit in Energy Metabolism Caused by FH Loss in RPE Cells. Antioxidants (Basel, Switzerland). 2021 Dec;10(12).

59. Cox J, Mann M. MaxQuant enables high peptide identification rates, individualized p.p.b.-range mass accuracies and proteome-wide protein quantification. Nat Biotechnol [Internet]. 2008;26(12):1367–72. Available from: https://doi.org/10.1038/nbt.1511

60. Tyanova S, Temu T, Sinitcyn P, Carlson A, Hein MY, Geiger T, et al. The Perseus computational platform for comprehensive analysis of (prote)omics data. Nat Methods [Internet]. 2016;13(9):731–40. Available from: https://doi.org/10.1038/nmeth.3901

61. Armento A, Murali A, Marzi J, Arrango-Gonzalez B, Kilger E, Clark SJ, et al. FH loss in RPE cells causes retinal degeneration in a human RPE-porcine retinal explant co-culture model. bioRxiv [Internet]. 2021 Jan 1;2021.07.26.453778. Available from: http://biorxiv.org/content/early/2021/07/26/2021.07.26.453778.abstract

62. Gingras AC, Gygi SP, Raught B, Polakiewicz RD, Abraham RT, Hoekstra MF, et al. Regulation of 4E-BP1 phosphorylation: a novel two-step mechanism. Genes Dev. 1999 Jun;13(11):1422–37.

63. Chapman NA, Jacobs RJ, Braakhuis AJ. Role of diet and food intake in age-related macular degeneration: a systematic review. Clin Experiment Ophthalmol. 2019 Jan;47(1):106–27.

64. Felszeghy S, Viiri J, Paterno JJ, Hyttinen JMT, Koskela A, Chen M, et al. Loss of NRF-2 and PGC-1α genes leads to retinal pigment epithelium damage resembling dry age-related macular degeneration. Redox Biol. 2019 Jan;20:1–12.

65. Zhou Y, Zhou B, Pache L, Chang M, Khodabakhshi AH, Tanaseichuk O, et al. Metascape provides a biologist-oriented resource for the analysis of systems-level datasets. Nat Commun. 2019 Apr;10(1):1523.

66. Fleckenstein M, Keenan TDL, Guymer RH, Chakravarthy U, Schmitz-Valckenberg S, Klaver CC, et al. Age-related macular degeneration. Nat Rev Dis Prim. 2021 May;7(1):31.

67. Strunz T, Kiel C, Sauerbeck BL, Weber BHF. Learning from Fifteen Years of Genome-Wide Association Studies in Age-Related Macular Degeneration. Cells. 2020 Oct;9(10).

68. Ormsby RJ, Ranganathan S, Tong JC, Griggs KM, Dimasi DP, Hewitt AW, et al. Functional and structural implications of the complement factor H Y402H polymorphism associated with age-related macular degeneration. Invest Ophthalmol Vis Sci. 2008 May;49(5):1763–70.

69. Laine M, Jarva H, Seitsonen S, Haapasalo K, Lehtinen MJ, Lindeman N, et al. Y402H polymorphism of complement factor H affects binding affinity to C-reactive protein. J Immunol. 2007 Mar;178(6):3831–6.

70. Truillet C, Cunningham JT, Parker MFL, Huynh LT, Conn CS, Ruggero D, et al. Noninvasive Measurement of mTORC1 Signaling with (89)Zr-Transferrin. Clin cancer Res an Off J Am Assoc Cancer Res. 2017 Jun;23(12):3045–52.

71. Ikenoue T, Hong S, Inoki K. Monitoring mammalian target of rapamycin (mTOR) activity. Methods Enzymol. 2009;452:165–80.

72. Datta SR, Brunet A, Greenberg ME. Cellular survival: a play in three Akts. Genes Dev. 1999 Nov;13(22):2905–27.

73. Yang W-L, Wu C-Y, Wu J, Lin H-K. Regulation of Akt signaling activation by ubiquitination. Cell Cycle. 2010 Feb;9(3):487–97.

74. Rosner M, Siegel N, Valli A, Fuchs C, Hengstschläger M. mTOR phosphorylated at S2448 binds to raptor and rictor. Amino Acids. 2010 Jan;38(1):223–8.

75. Livingstone M, Bidinosti M. Rapamycin-insensitive mTORC1 activity controls eIF4E:4E-BP1 binding. F1000Research. 2012;1:4.

76. Ruvinsky I, Meyuhas O. Ribosomal protein S6 phosphorylation: from protein synthesis to cell size. Trends Biochem Sci. 2006 Jun;31(6):342–8.

77. Choo AY, Yoon S-O, Kim SG, Roux PP, Blenis J. Rapamycin differentially inhibits S6Ks and 4E-BP1 to mediate cell-type-specific repression of mRNA translation. Proc Natl Acad Sci U S A. 2008 Nov;105(45):17414–9.

78. Dennis PB, Pullen N, Kozma SC, Thomas G. The principal rapamycin-sensitive p70(s6k) phosphorylation sites, T-229 and T-389, are differentially regulated by rapamycin-insensitive kinase kinases. Mol Cell Biol. 1996 Nov;16(11):6242–51.

79. Wang Y, Chen Z, Jia C, Bai X, Jiang Y, Zou Z. Analysis of the mTOR Interactome using SILAC technology revealed NICE-4 as a novel regulator of mTORC1 activity. Life Sci. 2021 Sep;281:119745.

80. Feher J, Kovacs I, Artico M, Cavallotti C, Papale A, Balacco Gabrieli C. Mitochondrial alterations of retinal pigment epithelium in age-related macular degeneration. Neurobiol Aging. 2006 Jul;27(7):983–93.

81. Chiu C-J, Chang M-L, Zhang FF, Li T, Gensler G, Schleicher M, et al. The relationship of major American dietary patterns to age-related macular degeneration. Am J Ophthalmol. 2014 Jul;158(1):118-127.e1.

82. Zhao C, Yasumura D, Li X, Matthes M, Lloyd M, Nielsen G, et al. mTOR-mediated dedifferentiation of the retinal pigment epithelium initiates photoreceptor degeneration in mice. J Clin Invest. 2011 Jan;121(1):369–83.

83. Gensler G, Clemons TE, Domalpally A, Danis RP, Blodi B, Wells J, et al. Treatment of Geographic Atrophy with Intravitreal Sirolimus: The Age-Related Eye Disease Study 2 Ancillary Study. Ophthalmol Retin [Internet]. 2018;2(5):441–50. Available from: https://www.sciencedirect.com/science/article/pii/S2468653017302944

84. Clark SJ, Perveen R, Hakobyan S, Morgan BP, Sim RB, Bishop PN, et al. Impaired binding of the age-related macular degeneration-associated complement factor H 402H allotype to Bruch's membrane in human retina. J Biol Chem. 2010 Sep;285(39):30192–202.

85. Wyatt MK, Tsai J-Y, Mishra S, Campos M, Jaworski C, Fariss RN, et al. Interaction of complement factor h and fibulin3 in age-related macular degeneration. PLoS One. 2013;8(6):e68088.

86. Kleiger G, Mayor T. Perilous journey: a tour of the ubiquitin-proteasome system. Trends Cell Biol. 2014 Jun;24(6):352–9.

87. Kocaturk NM, Gozuacik D. Crosstalk Between Mammalian Autophagy and the Ubiquitin-Proteasome System. Front cell Dev Biol. 2018;6:128.

88. Klionsky DJ, Emr SD. Autophagy as a regulated pathway of cellular degradation. Science. 2000 Dec;290(5497):1717–21.

89. Wu WKK, Wu YC, Yu L, Li ZJ, Sung JJY, Cho CH. Induction of autophagy by proteasome inhibitor is associated with proliferative arrest in colon cancer cells. Biochem Biophys Res Commun. 2008 Sep;374(2):258–63.

90. Selimovic D, Porzig BBOW, El-Khattouti A, Badura HE, Ahmad M, Ghanjati F, et al. Bortezomib/proteasome inhibitor triggers both apoptosis and autophagy-dependent pathways in melanoma cells. Cell Signal. 2013 Jan;25(1):308–18.

91. Korolchuk VI, Mansilla A, Menzies FM, Rubinsztein DC. Autophagy inhibition compromises degradation of ubiquitin-proteasome pathway substrates. Mol Cell. 2009 Feb;33(4):517–27.

92. Zhan J, He J, Zhou Y, Wu M, Liu Y, Shang F, et al. Crosstalk Between the Autophagy-Lysosome Pathway and the Ubiquitin-Proteasome Pathway in Retinal Pigment Epithelial Cells. Curr Mol Med. 2016;16(5):487–95.

93. Zhao J, Zhai B, Gygi SP, Goldberg AL. mTOR inhibition activates overall protein degradation by the ubiquitin proteasome system as well as by autophagy. Proc Natl Acad Sci [Internet]. 2015 Dec 29;112(52):15790 LP – 15797. Available from: http://www.pnas.org/content/112/52/15790.abstract

94. Zhao J, Goldberg AL. Coordinate regulation of autophagy and the ubiquitin proteasome system by MTOR. Autophagy. 2016 Oct;12(10):1967–70.

95. Mitter SK, Song C, Qi X, Mao H, Rao H, Akin D, et al. Dysregulated autophagy in the RPE is associated with increased susceptibility to oxidative stress and AMD. Autophagy. 2014;10(11):1989–2005.

96. Zhang Z-Y, Bao X-L, Cong Y-Y, Fan B, Li G-Y. Autophagy in Age-Related Macular Degeneration: A Regulatory Mechanism of Oxidative Stress. Oxid Med Cell Longev. 2020;2020:2896036.

97. Liu Z, Qin T, Zhou J, Taylor A, Sparrow JR, Shang F. Impairment of the ubiquitin-proteasome pathway in RPE alters the expression of inflammation related genes. Adv Exp Med Biol. 2014;801:237–50.

98. Knudsen ES, Nambiar R, Rosario SR, Smiraglia DJ, Goodrich DW, Witkiewicz AK. Pan-cancer molecular analysis of the RB tumor suppressor pathway. Commun Biol [Internet]. 2020;3(1):158. Available from: https://doi.org/10.1038/s42003-020-0873-9

99. Nicolay BN, Danielian PS, Haas W, Stephanopoulos G, Lees JA, Dyson NJ. Metabolic analysis of the loss of Rb1 in vivo. Cancer Metab [Internet]. 2014;2(1):O4. Available from: https://doi.org/10.1186/2049-3002-2-S1-O4

100. Nicolay BN, Danielian PS, Kottakis F, Lapek JDJ, Sanidas I, Miles WO, et al. Proteomic analysis of pRb loss highlights a signature of decreased mitochondrial oxidative phosphorylation. Genes Dev. 2015 Sep;29(17):1875–89.

101. Blasiak J, Piechota M, Pawlowska E, Szatkowska M, Sikora E, Kaarniranta K. Cellular Senescence in Age-Related Macular Degeneration: Can Autophagy and DNA Damage Response Play a Role? Oxid Med Cell Longev. 2017;2017:5293258.

7 Declaration of own contribution

This thesis was conducted at the institute for ophthalmic research Tübingen under the supervision of Prof. Marius Ueffing and Dr. Angela Armento. This is to certify that I, David Adrian Merle, conducted most of the work associated with this thesis. The conception of the project took place in close cooperation between Prof. Ueffing, Dr. Armento and me. Dr. Armento supervised my laboratory work and provided me with all relevant protocols. I independently carried out all of the presented experiments, except the seahorse measurements, which were done by members of Prof. Michaela Deleidi's group (DZNE). All statistical analyses were performed by me under the supervision of Dr. Armento. For the biostatistical analysis of the mass spectrometry experiments, I received help from Dr. Mohamed Ali Jarboui, a senior member of Prof. Ueffing's group. I wrote the thesis without any external help and received input from Prof. Ueffing and Dr. Armento.

The results of this project were published in the peer-reviewed journal *Antioxidants* (58). Therefore, some parts of this thesis correspond to the published article. Relevant passages are marked and references to the article were included at all relevant instances. I assure that I created this thesis independently, without any external help and used no other than the referenced sources.

Tübingen, den 23.05.2023

David Adrian Merle

8 Publications

Parts of this thesis were published in:

Merle DA, Provenzano F, Jarboui MA, Kilger E, Clark SJ, Deleidi M, Armento A, Ueffing M. mTOR Inhibition via Rapamycin Treatment Partially Reverts the Deficit in Energy Metabolism Caused by FH Loss in RPE Cells. Antioxidants (Basel). 2021 Dec 3;10(12):1944. doi: 10.3390/antiox10121944. PMID: 34943047; PMCID: PMC8750186.